Solid-state NMR spectroscopy insights for resolving different water pools in alginate hydrogels

El Hariri El Nokab, Mustapha; Lasorsa, Alessia; Sebakhy, Khaled O; Picchioni, Francesco; van der Wel, Patrick

Published in:
Food hydrocolloids

DOI:
10.1016/j.foodhyd.2022.107500

Publication date:
2022

Food Hydrocolloids 127 (2022) 107500

Contents lists available at ScienceDirect

Food Hydrocolloids

journal homepage: www.elsevier.com/locate/foodhyd

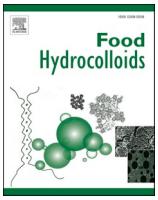

Solid-state NMR spectroscopy insights for resolving different water pools in alginate hydrogels

Mustapha El Hariri El Nokab [a], Alessia Lasorsa [a], Khaled O. Sebakhy [b], Francesco Picchioni [b], Patrick C.A. van der Wel [a,*]

[a] Zernike Institute for Advanced Materials, University of Groningen, Nijenborgh 4, 9747 AG, Groningen, the Netherlands
[b] Engineering and Technology Institute Groningen, University of Groningen, Nijenborgh 4, 9747 AG, Groningen, the Netherlands

ARTICLE INFO

Keywords:
Solid-state NMR spectroscopy
Alginate
Water phases
Water-biopolymer interactions
Drug delivery

ABSTRACT

Alginate hydrogels are versatile self-assembling biocompatible materials with diverse biomedical and food industrial applications, which includes uses in encapsulation, (drug) delivery and tissue engineering. Hydrogel formation requires cross-linking, which for alginates is often done with calcium ions that engage in specific interactions with the polysaccharide carboxylic acid groups. Water molecules also hydrate these alginate groups and fill macropores within the hydrogels, with implications for both mechanical properties and cargo encapsulation. Understanding these aspects of hydrogels requires the observation and characterization of the hydrogel waters, how they engage the alginate, and fill the macropores. Here we employed solid-state NMR (ssNMR) spectroscopy to detect and study water molecules in re-hydrated alginate hydrogels. ^{1}H, ^{2}H, and ^{13}C magic angle spinning (MAS) NMR and relaxation measurements were combined to observe both water and alginate. Two different water phases were detected that vary upon gradual (re)hydration of the alginate hydrogels. These water pools differ in their chemical shifts and NMR relaxation properties, reflecting hydration waters directly associated with the carbohydrate polymers alongside dynamic waters in the macropores. Thus, the ssNMR detects the water-filled macropore water pools and how they vary upon calcium cross-linking. We also observe how calcium cross-linking selectively immobilizes the α-guluronate monosaccharides, but leaves the β-mannuronate units more flexible and prone to selective re-hydration. Thus, these ssNMR experiments can be used to probe cross-linking and hydration of alginate hydrogels, with implications for our understanding of design parameters that tune their performance in (drug) delivery and other food industrial applications.

1. Introduction

Hydrogels are hydrophilic three-dimensional interpenetrating networks comprised of cross-linked nanofibrous materials (Chai et al., 2017). They can be assembled from natural or synthetic polymers or a mixture of both. A remarkable feature of many hydrogels is that they absorb and retain large amounts of water, even thousands of times their own dried weight, while remaining insoluble and preserving their structural and dimensionally constrained integrity (Chivers & Smith, 2019). A hydrogel's properties naturally depend on the characteristics of the nanofibers (or polymers) that are its fundamental building blocks. Moreover, by tuning the extent and nature of the cross-links between those constituent nanofibers one can influence the performance and functionality of the hydrogel (Pescosolido et al., 2012; Raghuwanshi & Garnier, 2019). When hydrogels are formed via *covalent* cross-links, they are known as permanent or chemically stable hydrogels. Alternatively, in reversible or physically stable hydrogels the polymers are cross-linked via non-covalent interactions, which include molecular entanglements, ionic forces, hydrogen bonds, Van der Waals and π-π stacking interactions (Campoccia, 1998; Prestwich et al., 1998). A notable functional feature of the latter class of hydrogels is that they may disassemble or disintegrate upon exposure to external stimuli, enabling the design of responsive hydrogels with a wide range of potential applications, including biomedical and food related uses such as spatially or temporally controlled drug and bioactive compound delivery (Bennacef et al., 2021; Chen, 2018; Kühn et al., 2016; Lin et al., 2019; Matera et al., 2019; Santos & Garcia-Rojas, 2021).

Hydrogels are widely used in the food industry as biocompatible soft materials, with their chemical and structural versatility and high capacity of water swelling enabling the creation of many types of advanced

* Corresponding author.
E-mail address: p.c.a.van.der.wel@rug.nl (P.C.A. van der Wel).

https://doi.org/10.1016/j.foodhyd.2022.107500
Received 9 September 2021; Received in revised form 14 December 2021; Accepted 9 January 2022
Available online 13 January 2022

materials (Gun'ko et al., 2017). Moreover, the hydrogels' ability to (over time) degrade into physiological metabolites under particular conditions is important for medical applications such as drug delivery and regenerative medicine. For such applications, it is also beneficial to employ hydrogels that resemble natural extracellular matrices and cell adherence surfaces, e.g. to allow their deployment for cell proliferation (Dahlmann et al., 2013).

Of special interest are ionotropic hydrogels, which are non-covalently linked hydrogels that feature strong but reversible cross-links. These hydrogels form upon the combination of charged polyelectrolytes with multivalent ions or electrolytes with the opposite (counter) charge (Dompé et al., 2020), which can be responsive or "functional" based on their responsiveness to external stimuli (Hoffman, 2012). For biomedical and food industrial applications, highly charged (natural) polysaccharides are widely used for the design of ionotropic hydrogels, given their bio-compatibility and bio-degradability (Bennacef et al., 2021; Santos & Garcia-Rojas, 2021). Calcium alginate is a classic example that has been fabricated in capsule forms and stabilized with a complex coacervate coating to become an attractive tissue engineering matrix (Lim & Sun, 1980). Alginate is a polyanionic polymer (Fig. 1) obtained from various biological sources, based on a polysaccharide backbone of repeating units of 1,4-linked β-mannuronic acid (M) and α-guluronic acid (G) outfitted with carboxyl and hydroxyl functional groups (Fig. 1 (a,b)). Natural alginates consist of linear polysaccharide chains comprised of M and G homopolymeric blocks intermixed with MG heteropolymeric blocks (Lee & Mooney, 2012). Industrial alginate production was not only utilized by the food industry, but also for industrial and pharmaceutical applications. Applications in the pharmaceutical industry range from oral (Sosnik, 2014) or controlled release delivery (Tønnesen & Karlsen, 2002), to cancer treatment (Abasalizadeh, 2020), and protein and cell delivery (Lee and Mooney, 2012). Alginate hydrogels (Fig. 1 (c)) are also used as synthetic extracellular matrix materials in cell encapsulation, proliferation and transplantation applications (Andersen et al., 2015). A wide variety of chemical modifications (e.g. with polypeptides) can modulate the hydrogel elasticity, stiffness and stability and permit control over cell-matrix interactions (Khavari et al., 2016).

The chemical structure of cross-linked alginate, as well as its hydration properties, are of crucial importance for its deployment as an encapsulation or (controlled release) carrier system. Alginate's carboxyl and hydroxyl functional groups (Fig. 1 (a, b)) facilitate electrostatic and hydrogen bonding interactions with cargo, enabling control over their release (Lee & Mooney, 2012). In some designs, (drug) delivery systems contain drug reservoir compartments that are encapsulated with an alginate-based membrane barrier (Tønnesen and Karlsen, 2002). Then, upon exposure to a high level of hydration, the alginate molecules will reorganize into a high viscosity hydrocolloidal layer that retards and controls the migration of drugs (Tønnesen & Karlsen, 2002). Alternatively, in a polymer matrix system the cargo is dispersed within the (alginate-containing) matrix, and its release depends on the swelling of the hydrated bulk matrix, along with matrix erosion at the periphery. Optimal performance of the hydrogel for these various applications is tuned with parameters such as cross-linker type and concentration, but also the cross-link time (Takka et al., 1998; Wang & Spencer, 1998; Østberg et al., 1993).

Alginates can be cross-linked with different mono and divalent

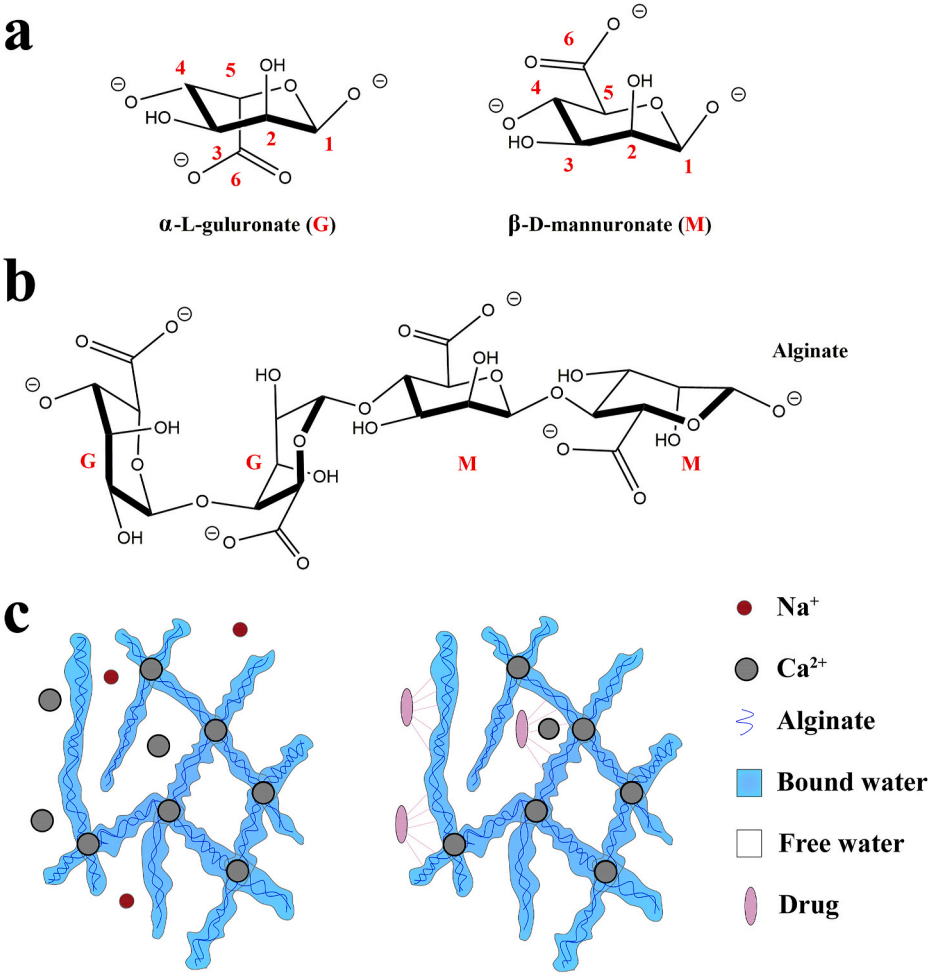

Fig. 1. Alginate's monosaccharide building blocks, polymer structure, and a hydrogel schematic representation. (a) α-L-guluronate (G) and β-D-mannuronate (M) are the monosaccharide constituents of alginate, (b) chemical structure of the linear alternating GG and MM blocks and heteropolymeric (MG) linkages in polymeric alginate. (c) Schematic drawing of interpenetrating alginate polymeric chains cross-linked by Ca^{2+} ions, without (left) and with (right) integrated drugs. See legend and text for explanation of hydrogel components.

cations and to a certain extent also with trivalent ions, resulting in hydrogels with different properties (Brus et al., 2017; Hu et al., 2021). Divalent calcium ions act as highly effective cross-links, through their preferential binding to G blocks, via a mechanism often described as the egg box model (Atkins et al., 1973; Braccini & Pérez, 2001; L.; Li, Fang, et al., 2007; Sikorski et al., 2007). The cross-linking procedure itself can be tuned based on the ratios of alginate to calcium, choice of alginate (with varying G/M composition), and cross-linking incubation time (Andersen et al., 2015; Hecht & Srebnik, 2016). Depending on the conditions and exact procedure, hydrogels with different cross-linking levels and thus different mesh sizes are obtained (Raghuwanshi & Garnier, 2019). These structural features dictate the mechanical properties of the hydrogel. Crucially, they also impact the macropore sizes, which are key for cargo encapsulation and delivery (Cuccia et al., 2020; Pescosolido et al., 2012).

These hydrogel parameters relate directly to its aqueous content. Water makes up a large part of the hydrogel, where it can be classified into strongly associated and weakly associated waters. This classification reflects the degree to which the water molecules associate directly with the alginate matrix through hydrogen bonding (Jhon & Andrade, 1973). A portion of the water molecules is engaged in extended interactions with alginate's hydrophilic groups, while other waters occupy the macropores where they move freely and only weakly interact with the polymers, during transient interactions. The latter macropore waters interact with encapsulated cargo, and also inform on the presence and size of the macropores. Detecting and studying these waters is therefore important. One way distinct types of hydrogel waters can be classified (and detected) is based on their freezing behavior, with water molecules in confined spaces and involved in strong hydrogen bonding to the polymer resisting freezing below 0 °C. This phenomenon is also seen in other (biological) contexts (Böckmann et al., 2009; Mandal & van der Wel, 2016). In hydrogels one can identify three types: (1) non-freezable water (which is strongly bound to alginate), (2) water with a freezing point similar to bulk water, and (3) water that experiences freezing point depression due to being constrained within the hydrogel (Gun'ko et al., 2017, 2007, 2005). Alternatively, hydrogel waters are also distinguishable by their dynamics: immobile water that is tightly bound to alginate, dynamic "free" water that is not bound, and water that has intermediate mobility due to transient or weak binding interactions (Sederel et al., 1983). In summary, "free" water is able to flow freely through or outside the matrix (tissue) unimpeded, with minimum interactions with the alginate itself (Penfield & Campbell, 1990; White et al., 2014). Bound water is defined as water held very tightly to the (alginate) matrix, rendering it generally immobile and resistant to freezing. With intermediate mobility, entrapped water is defined as water molecules that are encapsulated by the structural features of the matrix but have weaker or transient associations with the matrix. These water molecules experience a reduced level of mobility (compared to "free" water). Naturally, there can be exchange between distinct pools, dependent on the proximity and diffusion rates of the water pools (Penfield & Campbell, 1990; White et al., 2014). One useful aspect of the above is that structurally and functionally relevant parameters like the hydrogel mesh size and macropore size are reflected in the differing amounts of these distinct hydrogel waters, with macropores filled with encapsulated but not tightly bonded water molecules.

Detecting and quantifying such water pools, and how they are formed (e.g. upon re-hydration of lyophilized alginate nanoparticles) is therefore of significant interest and importance. In the current work we set out to study the water in rehydrated alginate hydrogels, both as a function of hydration level and cross-linking time. The study of hydrogel waters relies typically on an integration of multiple techniques, which can include differential scanning calorimetry (DSC) (Yoshida et al., 1993; Yudianti et al., 2009), small molecular probes (Amsden, 1998), X-ray powder diffraction (Naohara et al., 2017), dielectric relaxation spectroscopy (Kyritsis et al., 1995), thermally stimulated depolarization current (Gun'ko et al., 2007), quasi-elastic light scattering (Schmitz & Lu, 1983), diffusion and adsorption (Gun'ko et al., 2010; Savina et al., 2011), solution-state (Wende et al., 2020) and solid-state NMR (ssNMR) (Baumgartner et al., 2002), rheometry, and infrared spectroscopy (Pasqui et al., 2012). Each technique contributes a specific perspective with its own limitations.

Here we deployed a subset of these techniques to probe the interactions and behavior of water molecules in (re)hydrated and lyophilized hydrogels assembled by calcium cross-linking of alginate. We specifically looked at the distinction between encapsulated (macropore) water and alginate-associated water, how water molecules interact with specific groups in the alginate molecules, and how these features depend on the cross-linking time period use to prepare the lyophilized hydrogel. As a central tool we used magic angle spinning (MAS) ssNMR, based on its ability to provide information on the molecular and atomic level in a nondestructive fashion, not only for crystalline or dry samples, but also in disordered, amorphous and gel-like samples (Fu et al., 2011; Li, Xu, et al., 2007; van der Wel, 2017, 2018; Weingarth & Baldus, 2013). This has allowed its use as a powerful technique to probe polysaccharides (Gidley & Bociek, 1985; Gidley, 1992; Tang & Hills, 2003; White et al., 2014; Wang, Phyo, et al., 2016; Brus et al., 2017; El Hariri El Nokab & van der Wel, 2020; Poulhazan et al., 2021). SSNMR was also chosen based on its capability to detect and characterize solvent molecules, even within a supramolecular assembly, and reveal their dynamical properties (Böckmann et al., 2009; Capitani et al., 2001; Mandal et al., 2017; Radloff et al., 1996; Wang, Zhang, et al., 2016). ^{1}H and ^{2}H NMR can distinguish water molecules based on differences in their chemical shift, relaxation properties and (quadrupolar) order parameters (Friedline et al., 2014; Kaieda et al., 2013; Krivokhizhina & Wittebort, 2014; F.; Wang, Zhang, et al., 2016; Wang et al., 2017; Wende et al., 2020). Here, we combine these ssNMR techniques with other methods that include high-resolution transmission electron microscopy (HRTEM), thermogravimetric analysis (TGA), and dynamic light scattering (DLS). We examined lyophilized Ca cross-linked alginate hydrogels and their rehydration properties (Forgács et al., 2021). We observed the behavior of water molecules inside the nanofibrous structure of the hydrogel, which revealed two dominant types of water: water bound to the alginate alongside water undergoing (restricted) diffusion in the macropores. Hydration was found to mobilize specific parts of the alginate fibers, distinct from the Ca-cross-linking sites. The obtained data illuminate how the alginate polymeric chain is gradually hydrated and how the Ca^{2+}-based cross-linking impacts the hydration process, as a consequence of evolving cross-linking patterns during the latter.

2. Materials and methods

2.1. Alginate solution NMR characterization

Alginic acid sodium salt (CAS Number 9005-38-3) was obtained from Sigma Aldrich in powder form, with a specified viscosity ranging between 15 and 25 cps for a 1 alginate weight (wt.) % dispersion in purified water. NaOH and $CaCl_2$ were purchased from Sigma Aldrich and used as received (NaOH 98% and $CaCl_2$ 97% purity). Proton NMR analysis was done to determine the alginate composition. For the solution state NMR, 2 wt % of alginic acid was dissolved in D_2O-based NaOH (0.025M) solution, after which NMR measurement was done on a 500 MHz Varian Unity INOVA NMR at 95 °C. Alginic acid was completely dissolved in the solution and no partial acid hydrolysis was done or droplets of chelator solution were added to the sample before measuring. Single pulse experiments were performed using 5 s of relaxation delay, 2 s acquisition time and 64 scans. An exponential line broadening of 1.0 Hz and no zero filling was used. The M/G ratio was calculated according to the relative areas of the 3 signals in the anomeric region of alginate (A, B and C indicated in Fig. S1 in the Supplementary material) using the method of Grasdalen et al. (Grasdalen et al., 1979; Salomonsen et al., 2008). The integration areas were chosen to be from 5.18 to 4.96 ppm, 4.82–4.57 ppm and 4.55–4.38 ppm for A, B and C,

respectively. Briefly, the integrated intensities of regions A (5.18–4.96 ppm), B (4.82–4.57 ppm), and C (4.55–4.38 ppm) were determined in MestReNova 12.0 software.

2.2. Size exclusion chromatography (SEC)

The number average molecular weight (M_n) of the alginic acid (Fig. S2 (a) in the Supplementary material) was determined by aqueous gel permeation chromatography (GPC) using an Agilent 1200 system equipped with a differential refractive index (DRI) detector and Polymer Standard Service (PSS) column set (PSS SUPREMA 100 Å, 1000 Å, 3000 Å). A solution of 0.05 M $NaNO_3$ was used as mobile phase. The system temperature was regulated at 40 °C with a flow rate of 1 mL/min. The alginate sample was dissolved in the mobile phase (i.e., 6 mg dissolved in 2 ml 0.05 M $NaNO_3$), filtered using a glass syringe attached to a 0.45 μm Teflon filter, and injected into the columns. Data were analyzed using PSS winGPC UniChrom software.

2.3. Alginate cross-linking procedure

The following procedure was used to synthesize 2 alginate wt. % hydrogels: 0.1 g of alginic acid was dissolved in 3 ml of 0.025 M NaOH under vigorous stirring, then 2 ml of 0.018 M $CaCl_2$ was added under ambient condition and at neutral pH. Condensation occurs under ambient conditions after 5 min, yielding a gel that takes the shape of the container. No excess free water was observed. The gel was left for different periods (15 min, 6 and 48 h) to condense before freeze-drying the samples. All samples were frozen at −80 °C for 6 h and then lyophilized using a bench top freeze dryer (Martin Christ (Osterode am Harz, Germany) Alpha 2–4 LDplus), condenser temperature −80 °C, pressure 100 Pa. The lyophilization time was 48 h for all hydrogels to ensure that not only free water is lyophilized, but also bound water. Rehydration of the dried gels was done by the controlled addition of different amounts of 99.8% D_2O (Sigma). All samples were measured fresh upon rehydrating with D_2O; no incubation period was applied; only the rehydrated gels were vortexed for 5 min before measuring to ensure the complete homogenization (by naked eye) of the sample.

2.4. Light scattering analysis of particle sizes

Three alginate hydrogels were cross-linked with Ca^{2+} ions for different periods (15 min, 6 h and 48 h aging period), alongside a control alginate sample that was not cross-linked. Following a previously reported procedure (Smaniotto et al., 2020) for light scattering analysis of the hydrogel particle sizes, these preparations were carefully dehydrated by lyophilization. The resulting dry powders were rehydrated to a concentration of 0.33 mg/ml in deionized water under continuous stirring at 400 rpm in a water bath set at 80 °C. The obtained fluid gels were then withdrawn via a glass pipette, filtered through 0.45 μm Teflon Whatman filters and then added to separate polystyrene DLS cuvettes prior to the DLS measurements. The polydispersity index (PDI) for the particle size distribution was calculated from the standard deviation of the hypothetical Gaussian distribution (i.e. $PDI = \sigma^2/Z_D{}^2$, where σ^2 is the standard deviation and Z_D is the Z average mean size). Particle size distributions (PSDs) were determined using a Malvern Zetasizer Ultra (Malvern instruments, UK), utilizing a Non-Invasive Back-Scatter (NIBS) detector at 13^o and 173^o. The analysis was performed at temperatures of 10 °C and 27 °C. The cuvettes were allowed to reach the desired temperatures by setting an equilibration time of 2 min prior to the measurements. The DLS measurements were performed in triplicate on a single sample, with mean values of all three measurements reported in Table 1.

2.5. Thermogravimetric analysis on rehydrated Ca^{2+} cross-linked alginate

As described above, Ca^{2+} cross-linked alginate was prepared using 2 wt % calcium and a cross-linking time of 15 min, lyophilized and then rehydrated with D_2O. Thermal gravimetric analysis (TGA) (Fig. S2 (b)) was done using a PerkinElmer Thermogravimetric Analyzer TGA 4000, where the rehydrated Ca^{2+} cross-linked alginate sample was placed in an alumina crucible and the weight % loss was determined under N_2 atmosphere using the following programmed heating protocol: 5 °C/min sample heating for the first 10 min followed by 10 °C/min heating period for 10 min.

2.6. High-Resolution transmission electron microscopy (HRTEM)

A small quantity (0.1 mg) of powdered alginate (including alginic acid sodium salt (Fig. S3 (a)), dehydrated non-cross-linked alginate (Fig. S3 (b)) and dehydrated Ca^{2+} cross-linked alginates aged for 15 min (Fig. S3 (c)) and 48 h (Fig. S3 (d)) was hydrated in 100 mL 0.25 M NaOH solution. A pipette was then used to withdraw and deposit a drop of this sample on the high-resolution transmission electron microscopy (HRTEM) carbon grid sample holder. The drop was then allowed to dry depositing the powder particles on the grid holder. The HRTEM images were collected on an FEI Tecnai F20 FEG TEM using an accelerating voltage of 200 kV.

2.7. Solid state MAS NMR

For ssNMR studies, dry alginate or lyophilized Ca-cross-linked alginate were transferred into 4 mm Bruker-style zirconia MAS ssNMR rotors (Bruker Biospin and CortecNet) as dry powders. Other samples were studied in a rehydrated state: 100 mg of lyophilized hydrogels were rehydrated with a fixed amount of D_2O to achieve the specified hydration levels. The obtained (re)hydrated alginate hydrogels were then transferred using a spatula into Bruker MAS rotors. In all cases the rotors were closed with a Kel-F drivecap. In some cases, additional inserts were placed between the sample and the drive cap (as indicated in the Results section). The ssNMR was performed on a Bruker Avance Neo FT-NMR spectrometer equipped with a standard bore 14.1 T magnet and a 4 mm two-channel ^{1}H-X broadband CPMAS probe from Bruker Biospin. The corresponding Larmor frequencies were 600.130, 150.903 and 92.124 MHz for ^{1}H, ^{13}C and ^{2}H, respectively. ^{1}H and ^{13}C chemical shifts were referenced to aqueous DSS using the indirect method, by measuring adamantane ^{13}C signals, as described previously (Morcombe & Zilm, 2003). Detailed experimental parameters for each reported ssNMR dataset are included in Table S1 in the Supplementary material.

Single pulse experiments on ^{1}H were done using the following conditions: 74.6 kHz nutation frequency (3.375 us 90° pulse), 20 s repetition delay, 16 scans, 0.08 s acquisition time, 6 kHz MAS spinning frequency and temperature of 10 °C. Single pulse experiments on ^{2}H were done using the following conditions: 33.3 kHz nutation frequency, 3 s repetition delay, 16 scans, 1 s acquisition time, 6 kHz spinning frequency and temperature set to 0 °C. Hahn echo experiments on ^{1}H were done using the following conditions: 74.6 kHz nutation frequency, 10 s repetition delay, 128 scans, 0.08 s acquisition time, 10 kHz spinning frequency and temperature set to 27 °C. The echo time was rotor synchronized, and increased from 0 to 19.2 ms. Hahn echo experiments on ^{2}H were done using the following conditions: 33.33 kHz nutation frequency, 3 s repetition delay, 32 scans, 0.5 s acquisition time, 6 kHz spinning frequency and temperature set to 0 °C. The echo time was rotor synchronized, and increased from 0 to 32 ms. ^{1}H T_1 relaxation time measurements were done using the saturation recovery Bruker pulse program (satrect1), using d20 (delay in saturation pulse train) and L20 (number of pulses in saturation pulse train) 50 ms and 50 respectively. Tau (recovery delay) was varied from 50 μs to 90s and a nonlinear regression was carried out to fit the best T_1 values for each peak using

TopSpin 4.07. The ^{1}H nutation frequency was 50 kHz, repetition delay 3 s, number of scans 4, 0.08 s acquisition time, 10 kHz spinning frequency and temperature set to 27 °C.

^{13}C direct excitation experiments with high power ^{1}H decoupling were done using the following conditions: 50 kHz ^{13}C nutation frequency (5 μs 90° pulse), 4 s repetition delay, 4096 scans, 0.01 s acquisition time, 6 kHz spinning frequency and temperature set to 0 °C. During the acquisition time, proton TPPM decoupling was set at 50 kHz (Bennett et al., 1995; Scholz et al., 2009). ^{13}C–^{1}H 70–100 ramped MAS cross polarization (CP) ssNMR experiments were done using the following conditions: 4.5 ms contact time (dehydrated Ca^{2+} cross-linked alginate and alginic acid), 1.5, 4.5 and 6.5 ms contact time (rehydrated Ca^{2+} cross-linked alginate), 50 kHz nutation frequency for ^{13}C, 4 s repetition delay, 4096 scans, 0.007 s acquisition time, 6 kHz spinning frequency and measuring temperature at 0 °C. Proton TPPM decoupling at 50 kHz was used, in order to avoid excess sample heating.

The ssNMR spectra were processed using TopSpin 4.07, plotted using MestReNova 12.0 and (where applicable) deconvoluted using NMRPipe (Delaglio et al., 1995). ^{13}C 1D spectra were processed after the FID was zero-filled to a total of 26k points and with 250 Hz exponential linebroadening and ^{1}H spectra with 16k zerofilling and 10 Hz exponential linebroadening, unless indicated otherwise. Graphs were plotted and equations were fitted using Origin 8.1 and MathWorks MatLab.

3. Results

3.1. Monomeric and cross-linked alginate in liquid-state NMR

Prior to hydrogel assembly, the alginate starting material (derived from algae) was characterized by solution NMR (Fig. 2 (a)). Based on relative anomeric signal intensities the M/G molar ratio is calculated to be 1.0 (Fig. S1) (Grasdalen et al., 1979; Salomonsen et al., 2008). From the solution NMR spectra, the structural parameters of the alginate's block structure were determined to be $F_G = 0.50$, $F_M = 0.50$, $F_{GG} = 0.35$, F_{GM}=$F_{MG} = 0.16$ and $F_{MM} = 0.34$, with an estimated error of ±5%. Size exclusion chromatography (SEC) analysis (Fig. S2 (a)) indicated a weight-average molecular weight (M_n = 118000 g/mol, M_w = 430700 g/mol) and polydispersity index (PDI) of 3.65 for the alginate.

Next, calcium ions were added (at 2 wt %) to cross-link the alginate into a hydrogel. This resulted in a viscous semisolid gel state without excess water outside the gel (syneresis), which featured spherical aggregates in transmission electron microscopy (TEM) analysis (Fig. S3). Liquid-state NMR of this intact hydrogel (without hydrolysis) yielded ^{1}H spectra in which the resolution and sensitivity were lost (Fig. 2 (b)). This finding is typical of polysaccharide hydrogels, whose viscosity and rigidity prohibit good solution NMR spectra to be obtained (Gidley, 1992; El Hariri El Nokab & van der Wel, 2020). While better solution NMR data can be obtained by lowering the viscosity through acid hydrolysis, this approach destroys the structure of the hydrogel. Instead, MAS NMR can be used to probe the non-hydrolyzed hydrogel (Gidley & Bociek, 1985; Gidley, 1992; El Hariri El Nokab & van der Wel, 2020). In the sections below, we describe our use of a series of ssNMR experiments to probe alginate and alginate hydrogels, in both the dry (lyophilized) and (re)hydrated states, with the aim of examining the effects and process of hydrogel rehydration.

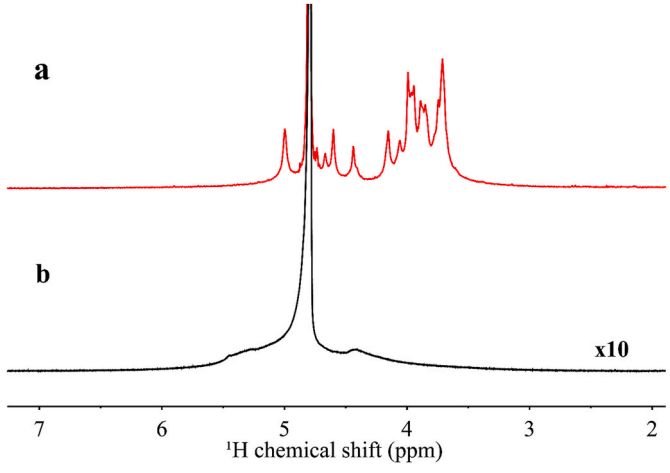

Fig. 2. ^{1}H solution state single pulse NMR experiments on dissolved alginic acid (Sol) and Ca^{2+} cross-linked alginate (Gel). (a) 2 wt % of alginic acid (purchased from Sigma) dissolved in D_2O-based NaOH (0.025M) solution. (b) Alginate cross-linked with calcium ions in the gel form. Both measurements were done on a 600 MHz Bruker NMR at 25 °C. Alginic acid was completely dissolved and no partial acid hydrolysis was done for either sample. Both spectra were referenced to the ^{1}H signal of residual H_2O at 4.79 ppm (room temperature).

3.2. MAS ssNMR of dehydrated alginate

First, MAS ssNMR was applied to the Ca^{2+} cross-linked alginate hydrogel that was lyophilized to dryness, alongside comparable measurements on the unlinked (dry) alginate starting material. The 1D ^{13}C cross-polarization (CP) MAS ssNMR spectrum for the starting material is shown in Fig. 3 (red lines). The alginate shows broad lines, reflecting the structural heterogeneity and lack of mobility of the dry polymer, consistent with prior reports (Salomonsen et al., 2008, 2009a, 2009b; Mollica et al., 2012). Based on published assignments and 2D ssNMR (Fig. S4) (Mollica et al., 2012; Salomonsen et al., 2008, 2009a, 2009b), specific ^{13}C peaks in Fig. 3 were assigned to carbons of the alginate using the nomenclature shown in Fig. 1. The anomeric carbons were observed between 60 and 110 ppm, while carboxyl carbons resonate near 180 ppm. ^{13}C signals from the M and G monosaccharides were distinguishable in the anomeric region, with their peaks having comparable intensities and linewidths. The black spectrum in Fig. 3 shows equivalent data for dry cross-linked alginate that had been submitted to 6 h of cross-linking with Ca^{2+} prior to lyophilization. As can be seen, the spectra for these dry samples were very similar, with only modest changes resulting from the cross-linking. The anomeric signals were largely unchanged in terms of their chemical shifts and linewidths. The most significant difference upon cross-linking was in the carbonyl region (160–190 ppm), where the cross-linked alginate gained a peak around 168–174 ppm, which matches the previously reported assignments for protonated carboxyl groups in alginate (Urbanova et al., 2019). We will now shift our focus to the impact and process of (re)hydration.

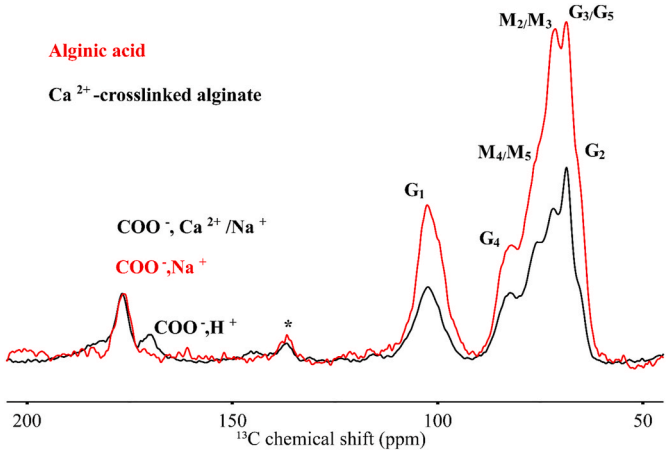

Fig. 3. 1D ^{13}C ssNMR spectra of dehydrated alginate in absence and presence of cross-links. ^{13}C–^{1}H 70–100 ramped MAS cross polarization (CP) ssNMR experiments were done on dehydrated Ca^{2+} cross-linked (6 h aged) alginate. The spectra were normalized to have the same intensity for carboxyl group. Asterisks mark spinning side bands.

3.3. ^{1}H and ^{2}H ssNMR showing controlled rehydration of Ca^{2+} cross-linked alginate

To characterize their rehydration behavior, we submitted the lyophilized Ca^{2+} cross-linked alginate to controlled hydration with D_2O, achieving hydration levels up to 77 wt. % D_2O (i.e., 23 wt. % alginate) (Forgács et al., 2021). For these experiments we prepared cross-linked hydrogel via 48 h of Ca^{2+} cross-linking, lyophilized the samples and back-added controlled amounts of D_2O, as specified. When these rehydrated samples were studied by thermogravimetric analysis (TGA), we observed that the bulk of the water is able to exit the alginate samples with relative ease, with no evidence of trapped water that resisted evaporation (Fig. S2 (b)).

We then used ^{13}C, ^{1}H and ^{2}H ssNMR to probe both solvent and alginate in the controlled rehydration samples. We first discuss the use of ^{1}H MAS ssNMR as it allowed us to see the hydration solvent directly, based on residual H_2O and HOD in the employed D_2O. The dry alginate and lyophilized hydrogels had very broad ^{1}H ssNMR spectra (Fig. 4a; Fig. S2 (c)) without the narrow peaks near 4–5 ppm expected for bulk water. Note that the corresponding (green) spectrum in Fig. 4a was so weak and broad that we show it 4x enlarged for clarity. Upon increasing the water content, we were clearly able to see the added solvent in the ^{1}H spectra (Fig. 4). Adding the smallest amount of D_2O (to achieve 62.5 wt% D_2O), the very broad peak observed for the dry material was dwarfed by a new peak at 5.1 ppm. Although much narrower than the signal for dry alginate, it was still fairly broad (163 Hz). We attributed this signal to the added water initially becoming hydration water that is engaged in specific interactions with the alginate. Upon adding more water (from 62.5 to 72.8 D_2O wt. %) we observed a similarly dominant peak, but this one was narrower and moved from 5.1 to 4.8 ppm. This chemical shift is closer to that of free water and the narrowing indicated an increase in mobility, both relative to the low-hydration sample. Further increasing the hydration level resulted in a ^{1}H peak with a sharp maximum at a slightly different chemical shift. Closer inspection (inset in Fig. 4 (a)) reveals that this was a peak with two constituent components: one that was identical to the signal seen at moderate hydration and one that was much narrower and resonated at 4.7 instead of 4.8 ppm. We attributed the narrow peak at 4.7 ppm to highly mobile water, whilst the broader 4.8 ppm peak was again water that was less mobile due to interactions with alginate functional groups. In other words, we saw two water environments with significantly different spectroscopic (NMR) characteristics: one narrow (15 Hz full width at half-height (FWHH)) and intense resonance near 4.7 ppm, and a broader resonance occurring at 5.1 to 4.8 ppm depending on the extent of hydration. Up to 62.5% we observed the water becoming engaged in alginate interactions, but at higher water levels the alginate functional groups became fully saturated such that traces of dynamic water started to appear.

Since the hydration was done with D_2O, we could also probe the solvent with ^{2}H MAS NMR (Fig. 4 (b)). Compared to the ^{1}H MAS NMR we did not observe as big a difference in the ^{2}H isotropic shift, such that the two water pools could now be distinguished primarily from differences in peak width. The width of the ^{2}H signals varied as a function of the hydration level. The hydrated alginate with 62.5 wt % D_2O showed the broadest peak having FWHH 1115 ± 5 Hz compared to 238 ± 5 Hz and 155 ± 5 Hz for 72.8 and 77 D_2O wt. %, respectively. Interestingly, the latter sample's peak width could be decreased further with a Hahn echo experiment (Fig. S5) when the echo time was 2.66 ms or longer.

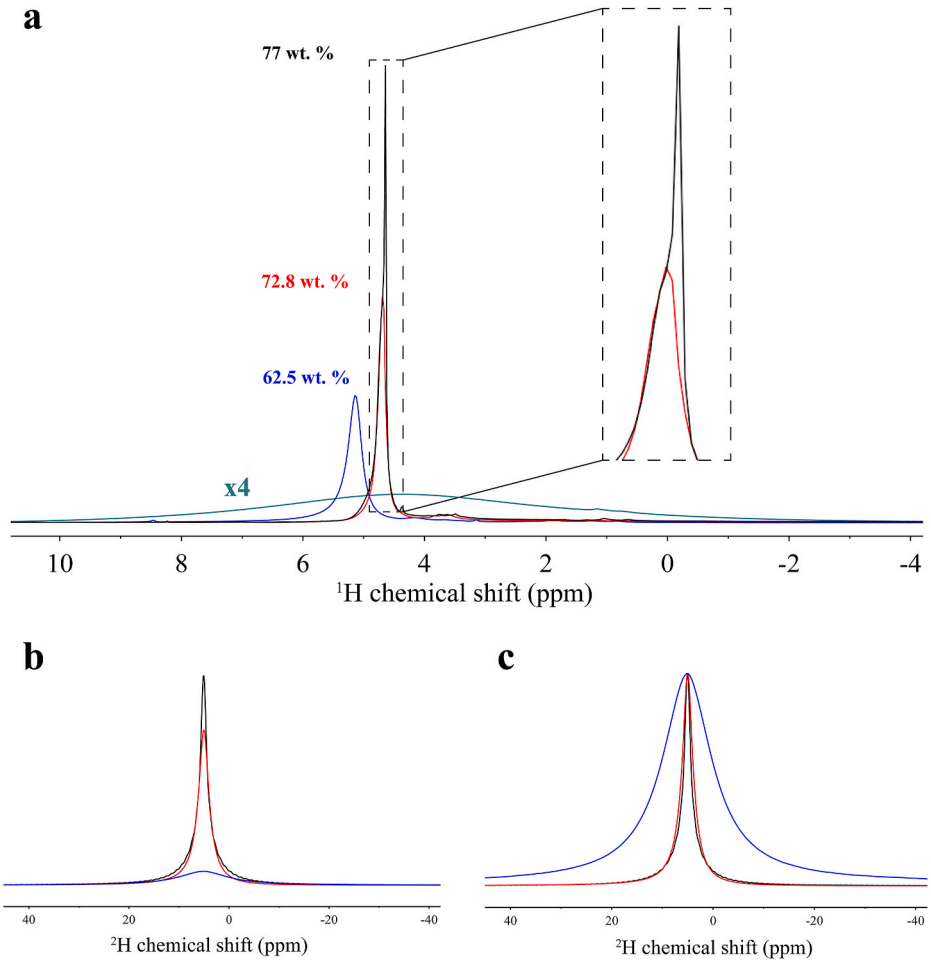

Fig. 4. ^{1}H and ^{2}H MAS single pulse NMR experiments for rehydrated Ca^{2+} cross-linked alginate. (a) Stacked ^{1}H spectra show dry alginic acid powder (green; 4x enlarged), and Ca^{2+} cross-linked alginate with increasing water content (62.5, 72.8 and 77 D_2O wt. %), as indicated. A bound water phase appears at the lowest level of hydration, followed by the increasing presence of the free water phase. Inset: Enlarged spectral region showing the overlapping components in the water signal for the two most hydrated preparations. All experiments were done at 600 MHz, using a 20 s repetition delay, 16 scans, 6 kHz spinning frequency and measuring temperature at 10 °C. (b) Stacked ^{2}H spectra show samples with the same increase of added water content, the bound water phase appears in a broad and low intensity signal followed by the free water phase which has sharp and high intensity signal. (c) Same spectra re-scaled to the peak maxima, to show linewidth changes. All experiments were done using a 3 s repetition delay, 16 scans, 6 kHz spinning frequency and measuring temperature at 0 °C. (For interpretation of the references to colour in this figure legend, the reader is referred to the Web version of this article.)

Then, the FWHH decreased from 155 ± 5 Hz (without echo) to 109 ± 5 Hz, due to the T_2 filter suppressing an underlying broader component from deuterated water with reduced mobility. Thus, also the ^{2}H NMR pointed to these hydrated hydrogels having distinct water pools with different mobility, analogous to the ^{1}H MAS NMR.

3.4. ^{13}C MAS NMR shows localized mobility in the rehydrated cross-linked alginate

We also probed the effect of the controlled rehydration on the cross-linked alginate itself, via ^{13}C-detected MAS NMR (Fig. 5). We saw already that ^{13}C MAS ssNMR of the lyophilized, cross-linked hydrogels gave broad ^{13}C CP MAS ssNMR spectra (Fig. 3), reflecting high sample heterogeneity and lack of motion. To look at the effect of hydration we turned to a slightly different MAS NMR experiment, based on ^{13}C direct excitation (DE) MAS NMR (Fig. 5(a and b)) as this experiment is useful for partly mobile samples (more below). Fig. 5 (a) shows the effect of increasing levels of rehydration (comparing to the dry alginate in Fig. 5 (b)). Two prominent peaks in the anomeric region stood out in the hydrated samples (marked with arrows). These signals represented specifically carbons of the M monosaccharides (Fig. 3), showing that there were clear hydration-dependent changes in these M-carbon signals. Even the lowest hydration level (62.5%) was found to be sufficient for the hydration of the M-carbon monosaccharides, where the G carbons remained unchanged. Subsequent increase of hydration until 77% lead only to the formation of bulk/free water filling the macropores of the hydrogels (see above), but with no further effect on the M-carbon peaks.

Here it is important to briefly discuss how these ssNMR techniques probe molecular- and atomic-level dynamics. ^{13}C DE ssNMR and ^{1}H–^{13}C CP ssNMR techniques probe the same ^{13}C sites, but give different peak intensities depending on sample mobility (Matlahov and Van der Wel, 2018). In CP ssNMR only those chemical groups that are rigid or semi-rigid show up, with the most rigid sites giving the most intensity, with some dependence on the CP contact time (Fig. 5 (c)). In DE ssNMR, we expect to see all sites (rigid and flexible alike), but with a bias toward more mobile groups when the recycle delay is kept relatively short (Fig. 5 (d)). Thus, any signals that were seen to be stronger in DE compared to CP spectra must be from flexible or dynamic parts of the sample. This effect is further enhanced when ^{1}H decoupling during acquisition is kept relatively low, as was done here (to minimize undesired RF-induced sample heating). In Fig. 5 (a), red arrows mark those peaks that were more intense and narrow in the DE ssNMR of the hydrated samples. These peaks were those of the COOH signals near 170 ppm and M monosaccharide carbons, previously assigned to M_2/M_3 at 71.6 ppm and M_4/M_5 at 76.4 ppm (Salomonsen et al., 2009a, 2009b). In other words, these M carbons became particularly mobile upon rehydration of the cross-linked alginate. We interpret this to indicate a preferential interaction of the M monosaccharide building blocks with the added water molecules.

Looking in more detail at the impact of varying the hydration levels in Fig. 5 (a), we observed that changes in the anomeric spectral region (60–120 ppm) were modest and difficult to interpret in detail. More striking is that the carboxyl group signal near 170 ppm varied in intensity. This signal thus appeared to be affected by interactions with increasing amounts of hydration water. In a comparison of CP- and DE-based spectra (Fig. 5 (c, d)) we observed that this peak is absent in the CP measurements. This chemical group was present (seen by DE ssNMR), but undetectable by CP ssNMR, which means the corresponding COOH group is dynamic. The conclusion that the ^{13}C DE spectra show more mobile carbonyl groups is also supported by the lack of the carboxyl spinning sidebands (* in Fig. 5 (b)), which in rigid samples reveals the large anisotropy of the carbonyl chemical shift. We also observed that in dry Ca^{2+} cross-linked alginate this COOH peak was near 170 ppm but upon rehydration it moved slightly and showed a narrower linewidth

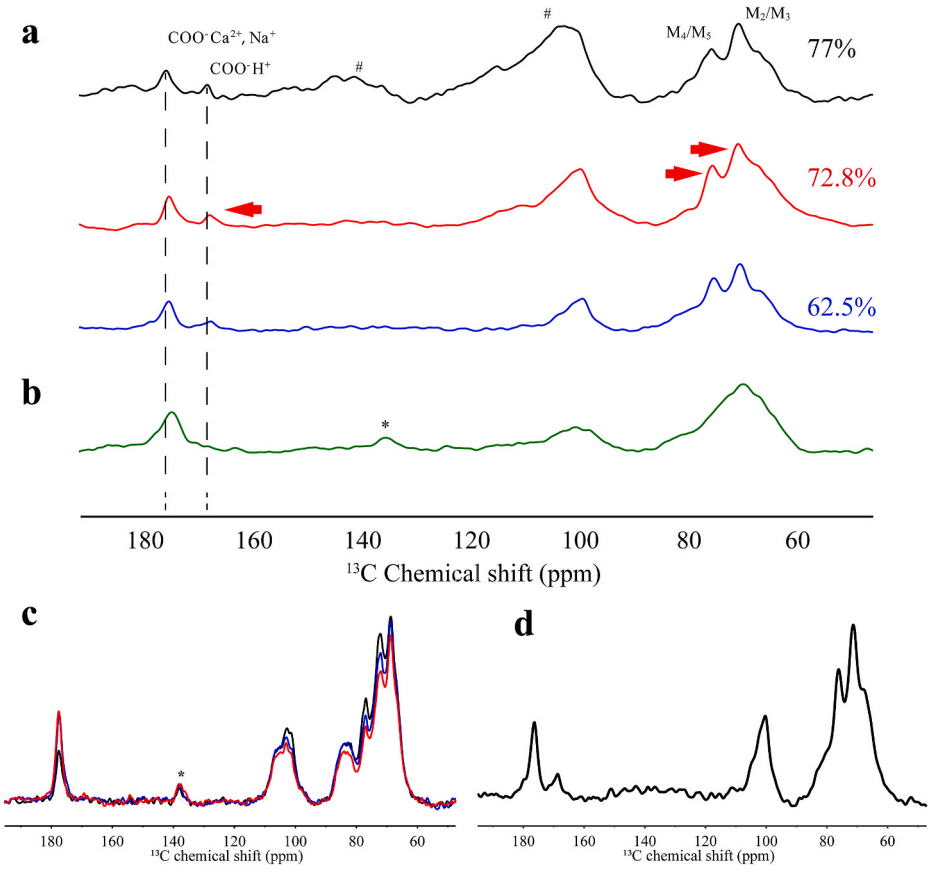

Fig. 5. ^{13}C MAS NMR of partly rehydrated 48 h Ca^{2+} cross-linked alginate. (a) ^{13}C direct excitation spectra of rehydrated Ca^{2+} cross-linked (48 h aged) alginate, hydrated with 77, 72.8 and 62.5 D_2O wt. %, as indicated. In the sample with 77% hydration a background signal from added sample spacers was detected and marked with #. Such spacers were omitted from the other samples. (b) Spectrum for dry alginic acid starting material powder. (c) 1D ^{13}C–^{1}H cross polarization (CP) ssNMR with varying contact times (1.5, 4.5, 6.5 ms; shown in black, blue, and red, respectively) for Ca^{2+} cross-linked (48 h) alginate in presence of 72.8 D_2O wt. %. (d) Direct excitation ^{13}C MAS NMR on the sample. Select assignments are indicated. All experiments were done using a 4-sec repetition delay, 4096 scans, 6 kHz spinning frequency and measuring temperature at 0 °C. Spinning side bands are marked with *. (For interpretation of the references to colour in this figure legend, the reader is referred to the Web version of this article.)

(FWHH 314 Hz). The signals of the main carboxyl (COO^-) functional groups also narrowed (the linewidth (FWHH) changes from 654 to 371 Hz) upon increasing the rehydration level and changed their resonance frequency from 176 to 177 ppm. These results indicated also that the exchange between the Na^+ and Ca^{2+} (counter)ions was successful (Brus et al., 2017; Urbanova et al., 2019). In summary, our ssNMR results revealed a preferential mobilization of the M monosaccharides upon rehydration, accompanied with a increased dynamics of carboxyl and COOH groups, with the COOH (near 170 ppm) becoming most flexible. Conversely, carbon sites associated with G monosaccharides were more rigid, reflecting more stable (and likely less hydrated) parts of the hydrogel structure.

3.5. Impact of Ca^{2+} cross-linking period of alginate hydrogel

We also studied the impact of the duration of the Ca^{2+}-induced cross-linking process (Lim & Sun, 1980). We performed DE ^{13}C MAS NMR spectroscopy on rehydrated alginate with the same water content (77 D_2O wt. %), but with increasing aging periods during the linking process before freeze drying (Fig. 6). All three samples were prepared according to the same procedure mentioned above, but with increasing aging period (15 min, 6 and 48 h) at ambient conditions *before* lyophilization. The 3 samples were then rehydrated with the same amount of D_2O (77 D_2O wt. %). Consistent with our earlier findings above, the distinct peak near the carboxyl region at 172 ppm (not seen in alginate starting material) increases in intensity with progressive Ca^{2+} cross-linking. Otherwise, the spectral changes are relatively modest.

More changes were seen when ^1H MAS NMR was used to probe the water dynamics in the same samples (Fig. 7). The broad ^1H peak observed at 4.8 ppm (attributed to immobilized bound water) decreases significantly while the narrow peak for free water at 4.7 ppm increases (Fig. 7 (a, b)). Quantitatively, the bound water signal varies from 78 to 46, and 48 %, for the samples aged from 15 min to 6 h and 48 h, respectively. Since all three samples contain the same amount of water (77 D_2O wt. %) and the only variable was the aging period, there is apparently an interconnection between the ratio of hydration water and free water, and the Ca^{2+} cross-linking time. The shift to more free water reflects the formation of more water in macropores with dynamical water molecules. On the other hand, the decrease in bound and immobilized water may reflect a competition between hydration and Ca-induced cross-linking. Consistent with the ^1H NMR data, ^2H MAS NMR experiments in Fig. 7 (c, d) reveal a significant decrease in the full line width at half height for aged rehydrated alginate gel from 155 Hz for sample aged for 15 min to reach 125 Hz for samples aged 6 and 48 h, respectively.

3.6. ^1H MAS NMR relaxation probes hydrogel water dynamics

The above ^1H MAS NMR studies provided a mostly qualitative analysis of the water phases, based on dynamic spectral editing methods. We also employed additional ssNMR experiments for a more in-depth study of the dynamic properties of the hydrogel waters. NMR relaxation rates depend on the molecular dynamics of the observed molecules and their environment. As such, relaxation measurements are powerful tools for studying water phases and their properties, and for determining the homogeneity of hydrogels (Böckmann et al., 2009; Capitani et al., 2001; Radloff et al., 1996). We applied ^1H T_1 relaxation MAS NMR measurements to distinguish different water phases in 15 min cross-linked alginate (Fig. 8). As shown in Fig. 8 (a), the shape of the ^1H-detected water peak was found to depend on the saturation recovery time. The broad component near 4.8 ppm showed a faster recovery and thus shorter T_1 relaxation time, compared to the narrow signal at 4.7 ppm. The distinct dynamic properties of these two water phases were confirmed by ^1H T_2 measurements (Fig. 8 (c)). Again, the broad and narrow signals have distinct properties. The broad signal decays faster (a shorter T_2), while the narrow signal decays much more slowly. The peak width in the ^1H 1D spectra is derived from a combination of homogeneous (T_2-based) and heterogeneous line broadening (Böckmann et al., 2009). The line widths of the narrow and broad signals are 17 and 118 Hz, respectively, consistent with their line widths being dominated by homogeneous effects. In summary, we observe a broad signal with short T_2 and short T_1, alongside a narrow peak with long T_2 and longer T_1. These findings are indicative of the narrow peak reflecting the highly dynamic "free" water phase, while the broader peak is due to partly immobilized hydration waters.

^1H NMR relaxation measurements were performed on the rehydrated

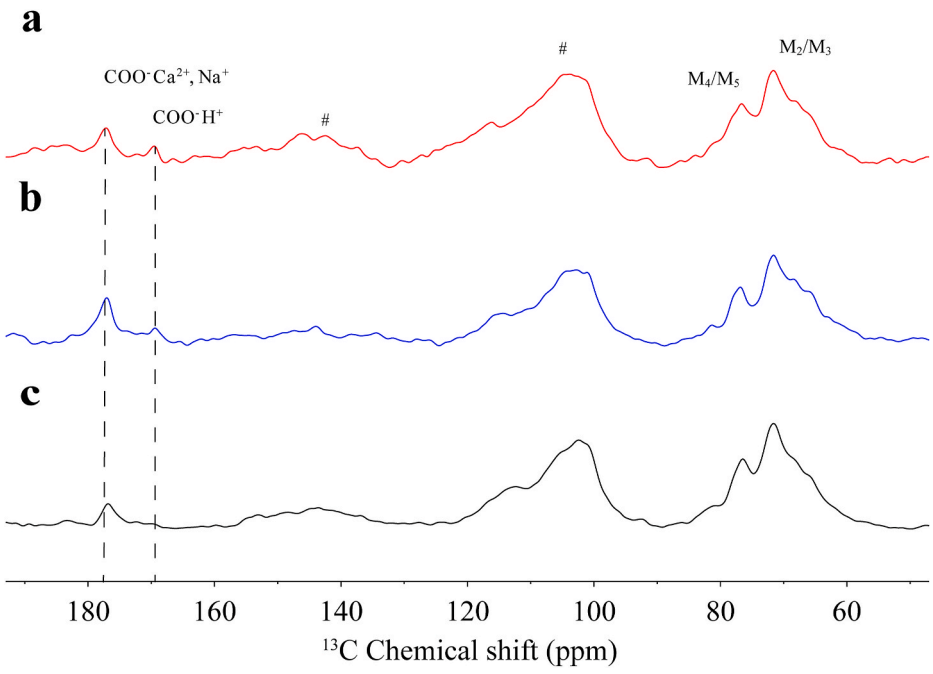

Fig. 6. DE ^{13}C MAS NMR for rehydrated Ca^{2+} cross-linked alginate (77 D_2O wt. %) with different aging periods. (a–b) Alginate Ca^{2+} cross-linked by 48 and 6 h, respectively. (c) Alginate treated with Ca for 15 min before freeze drying. Vertical dashed lines mark the C=O chemical shifts of protonated and non-protonated COO^- groups. All experiments were done using a 4 s repetition delay, 4096 scans, 6 kHz spinning frequency and a measuring temperature at 0 °C. Signals reflecting MAS spinning side bands are marked with asterisks (*), and background signals from sample inserts with #. The sample with 77% hydration level was outfitted with an insert, no other sample was measured with such a sample spacer.

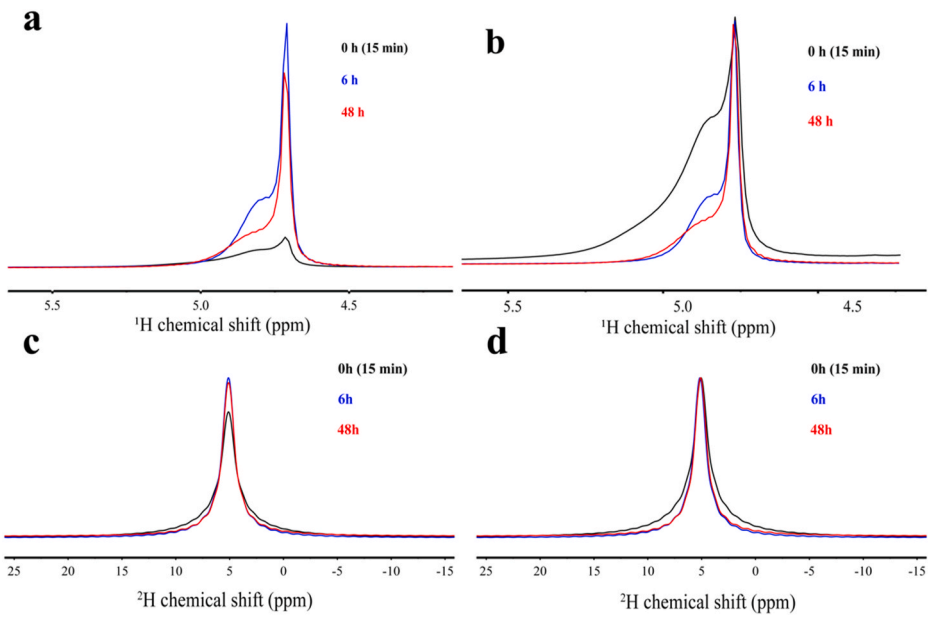

Fig. 7. ^{1}H and ^{2}H MAS single pulse NMR experiments for rehydrated Ca^{2+} cross-linked alginate. (a) ^{1}H MAS NMR spectra displayed with an absolute intensity scale. (b) The same data normalized to the highest peak, to enable comparison of the peak shapes. All three samples were prepared according to the same procedure with a varying aging period (15 min, 6 and 48 h) before lyophilization and subsequent rehydration with the same amount of D_2O (77 D_2O wt. %). All experiments were done using a 10-sec repetition delay, 128 scans, 10 kHz MAS frequency and measuring temperature of 27 °C. (c) ^{2}H MAS NMR spectra displayed with an absolute intensity scale. (d) The same data normalized to the highest peak, to enable comparison of the peak shapes. The width of the peak is significantly wider in the sample aged for 15 min (155 Hz) compared to the aged ones 6 and 48 h (125 Hz), respectively. All ^{2}H experiments were done using a 3 s repetition delay, 16 scans, 6 kHz spinning frequency and measuring temperature at 0 °C.

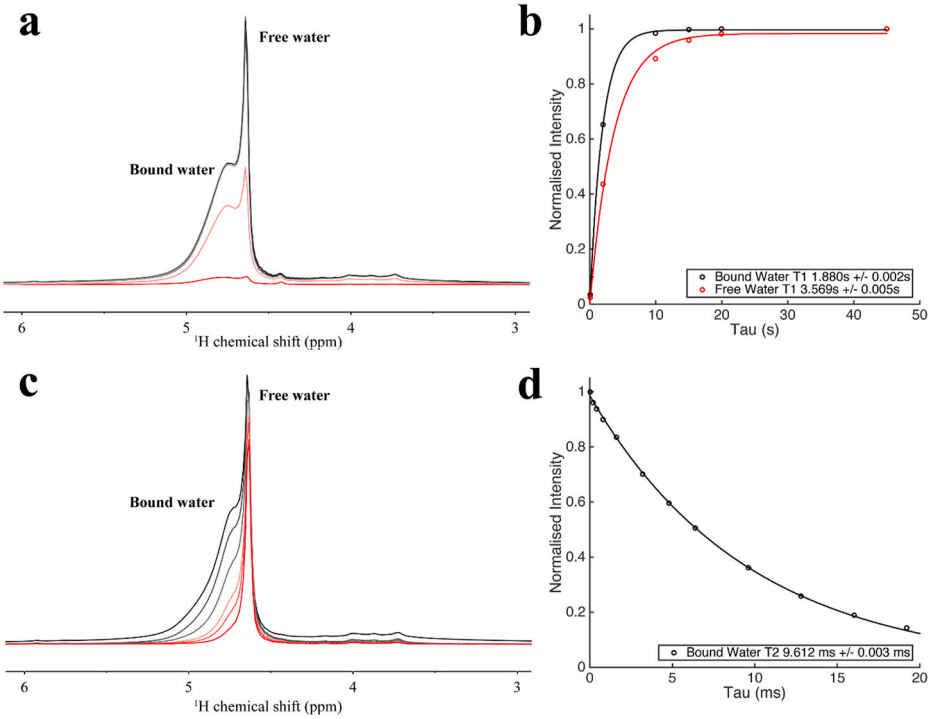

Fig. 8. MAS NMR relaxation measurements. (a) Saturation recovery ^{1}H NMR experiments done on rehydrated Ca^{2+} cross-linked alginate aged for 15 min showing the total recovery of the bound water signal to be faster than that of the free water, upon increasing the relaxation delays from 50 μs to 90 s. (b) Plot of peak intensity vs. relaxation delay τ for rehydrated Ca^{2+} cross-linked alginate aged for 15 min and the corresponding fit curves, (c) Hahn echo ^{1}H ssNMR experiments on rehydrated Ca^{2+} cross-linked alginate aged for 15 min, showing the total suppression of the bound water signal upon increasing the echo time from 0 to 19.2 ms. (d) Hahn echo decays measured for the broad component of the water peaks. All experiments were done using 10 kHz MAS frequency and a measuring temperature of 27 °C.

Ca^{2+} cross-linked alginate sample at 48 h aging (Fig. 9). Fitting reveals the T_1 values of broad signal to be $T_1 = 1.3 \pm 0.01$ s, whilst the narrow signal has $T_1 = 3.6 \pm 0.01$ s (Fig. 9 (a, b)). The distinct dynamic properties of these two types of water phases are also confirmed by ^{1}H T_2 measurements (Fig. 9 (c, d)). The line widths of the narrow and broad signals are 14 Hz and 79 Hz, respectively, consistent with the line width being dominated by homogeneous effects. Thus, again, the broad and narrow signals have distinct relaxation properties: a broad signal with short T_2 and short T_1, and a narrow peak with long T_2 and longer T_1. The comparison of the relaxational properties for the gels with different aging periods (15 min and 48 h) show an increase in the T_2 relaxational value for the bound water from 9.6 msec to 11.6 msec, which is reflected on the line width for the broad signal from 118 to 79 Hz for the 15 min aged gel and 48 h one, respectively. No significant changes appear on the T_2 relaxational values of the narrow signal or on the T_1 relaxational values of the aged gels.

An estimation of the rotational (re-orientational) correlation time can be obtained from the T_1/T_2 ratio (Kay et al., 1989). Since from our data it was not possible to extract a T_2 for free water, we used the value reported in a similar work done by Böckmann et al. (Böckmann et al., 2009). Based on the relaxational properties of the different water pools, we estimate at least an order of magnitude difference in the correlation time between the free and bound water pools.

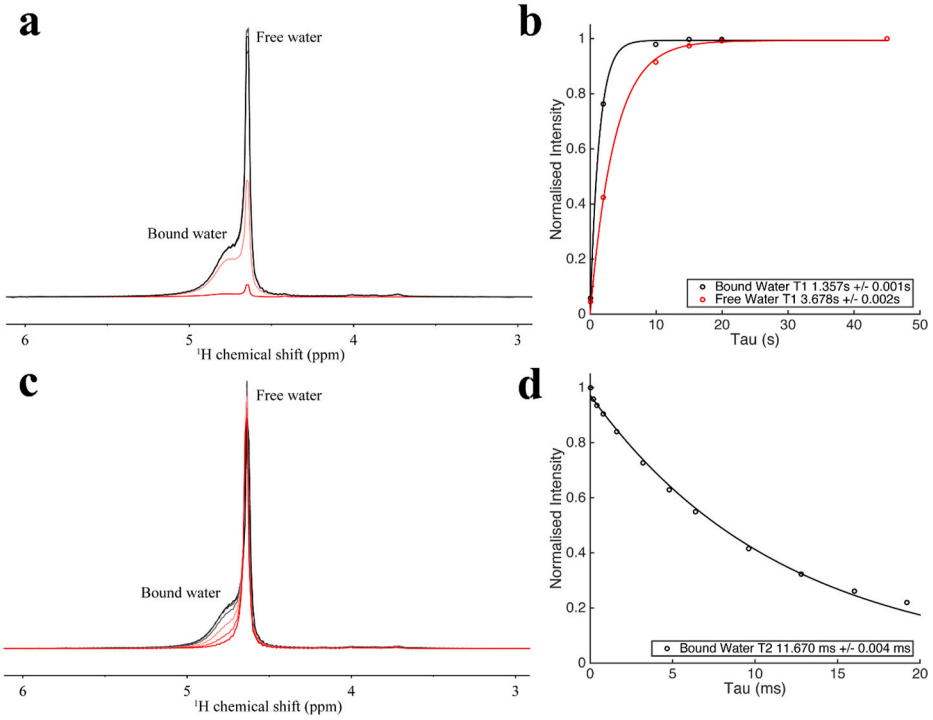

Fig. 9. MAS NMR relaxation measurements. (a) Saturation recovery ^{1}H NMR experiments done on rehydrated Ca^{2+} cross-linked alginate aged for 48 h showing the total recovery of the bound water signal to be faster than that of the free water upon increasing the relaxation delay from 50 μs to 90 s. (b) Plot of peak intensity vs. relaxation delay τ for rehydrated Ca^{2+} cross-linked alginate aged for 48 h and the corresponding fit curves. (c) Hahn echo ^{1}H ssNMR experiments on rehydrated Ca^{2+} cross-linked alginate aged for 48 h showing the total suppression of the bound water signal upon increasing the echo time from 0 to 19.2 ms. (d) Hahn echo decay measured for the broad component of the water ^{1}H peaks. All experiments were done using 10 kHz MAS frequency and measuring temperature of 27 °C.

3.7. Particle size distribution of aged alginate

The ssNMR analysis provides a molecular level perspective, but does not directly probe the overall structure of the cross-linked hydrogel. To examine this aspect we also analyzed the particle size distribution (PSD) of our preparations, revealing the size of the cross-linked nanoparticles within the lyophilized hydrogel and their homogeneity. The PSD is not expected to be significantly affected by the freeze drying process (Smaniotto et al., 2020), although there may be a disruption of weak or temporary Ca^{2+} cross-links, an expansion of certain short-range ordered structures during dehydration, and a shrinking of the overall polymer network (Naohara et al., 2017). The lyophilized powders were first completely dissolved in solvent for PSD measurements at 10 and 27 °C, based on light scattering analysis. Figs. 10 and S2 (d) and Table 1 show the PSDs of the three alginate gels cross-linked for different periods (15 min, 6 h, and 48 h). For the shortest cross-linking period the mean average particle diameter was found to be around 72 nm (Smaniotto et al., 2020). When the samples were aged longer, the mean average particle diameter decreased to 41 nm and 35 nm, for 6 h and 48 h of aging. At 27 °C the mean average particle diameter for the 15 min cross-linked sample was found to be around 92 nm, indicating an increased level of aggregation. It is worthwhile to mention that these two aged samples exhibited a narrower particle size distribution than the starting material (Figs. 10 and S2 (d)). Thus, increasing the Ca cross-linking time yields increasingly compact and homogeneous nanoparticles, on the 40–100 nm scale.

Table 1
Particle size distribution results as a function of cross-linking period for rehydrated Ca^{2+} cross-linked alginate, averaged from three separate measurements.

Sample	D (nm)	PDI
15 min	72	0.38
6 h	41	0.46
48 h	35	0.47

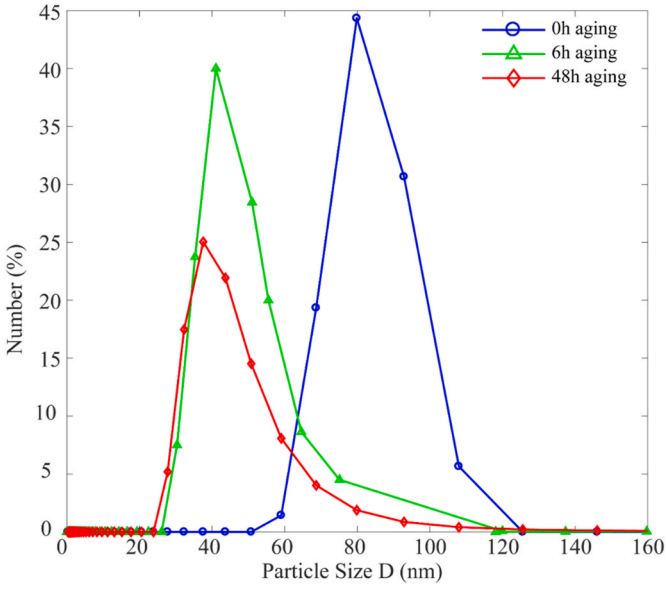

Fig. 10. PSDs at 10 °C of different alginate gels produced at different aging periods. Lyophilized Ca^{2+}-cross-linked alginate was obtained after different cross-linking periods (0h (15 min), 6 and 48 h) and analyzed in triplicate. Representative results from a single measurement are shown here, with the averaged values reported in Table 1.

4. Discussion

4.1. Hydration of Ca^{2+} cross-linked and non cross-linked alginate

By ssNMR we observed structural and dynamic changes that accompany the hydration of alginate in presence and absence of Ca cross-links, as visualized in Fig. 11 (a). We observed the presence of two dominant distinct water phases within the alginate hydrogel, with significantly different spectroscopic, dynamic, and relaxation properties. TGA showed the hydrogel to be very open, with porous macropores, and gave no evidence of trapped or encapsulated water. Thus, these distinct hydration pools must be connected but nonetheless endowed with distinct properties. Accordingly, we attributed the water resonances to semi-free water in macropores and alginate-associated water that interacts with the hydrogel matrix, respectively (Fig. 11 (a)). With multiple MAS NMR experiments, we observed clear differences in ^{1}H and ^{2}H spectra, in terms of linewidths for the respective water pools. Explicit relaxation measurements showed that these linewidth differences originated from dynamic differences, informing the above-mentioned attribution to macropore and hydration water.

In parallel, we employed ^{13}C NMR to monitor the impact of hydration and cross-linking on the alginate itself. Notably, we observed selective and localized effects, in which particular signals from the M monosaccharide were impacted by the lower hydration levels. This was apparent from the narrowing of M carbon signals in DE excitation spectra shown in Fig. 5, relative to both dry samples and CP-based spectra. Given the distinct dynamic spectral editing (DYSE) properties (Matlahov & van der Wel, 2018) of these types of ssNMR spectra, we must conclude that hydration selectively mobilizes these M carbon sites. These data showed that the hydration process does not equally affect all of the alginate, but rather leads to dominant changes in the M monosaccharide. This is evident in spectra in Fig. 5, showing a prominent change in the peaks of M. These findings are consistent with published data on alginate hydration (Chan et al., 2007). The preferential hydration of M may be explained by the chemical structure of these monosaccharide blocks, but the M and G groups are chemically very similar. Instead, it is more easily explained with reference to the popular egg-box model of how Ca^{2+} ions facilitate hydrogel cross-linking in alginate. This well-known egg-box model of alginate hydrogel formation (Atkins et al., 1973; Braccini & Pérez, 2001; L.; Li, Fang, et al., 2007; Sikorski et al., 2007) involves the formation of G-Ca clusters upon addition of Ca^{2+}, leading to Ca-mediated cross-links between alginate polymers. This could be expected to yield immobile cross-link clusters involving the G blocks, which are not only inherently rigid but also appear to resist re-hydration. Accordingly, our data show that the M sites are less impacted by Ca cross-linking and also preferentially "mobilized" during the controlled hydration process. It is therefore also tempting to speculate that the characteristic carboxyl group signals that are observed to become increasingly mobile when hydrating the Ca-cross-linked alginate are largely due to these hydrated M groups. We noted several lines of evidence for the presence of more dynamic and more rigid carboxylic acid groups in these samples. This included their detection in the DE or CP-based ssNMR (Fig. 5), the relative linewidths, as well as the presence and absence of MAS-related spinning side bands. Based on all these data, the partly hydrated alginate hydrogels feature both rigid and mobile carboxyl groups, with the more mobile ones most likely associated with M groups given the analogous dynamics to the more-easily-recognized aliphatic M carbons.

We also obtained insights into the impact of extended cross-linking periods. From particle size analysis it was seen that large particles were formed early on, but that these restructured into more compact nanoparticles as cross-linking time increased. In parallel, the ^{1}H NMR data showed a shift from mostly hydration of the alginate (immobilized water molecules) to more and more mobile water, present in macropores in the hydrogel. We reconcile these data with a model in which the sudden introduction of Ca^{2+} ions into the solution of sodium alginate, leads to large particle size aggregates in which much of the alginates are accessible to hydration, but few macropores are formed. Upon increasing the Ca^{2+} cross-linking time the hydrogel undergoes a gradual restructuring toward a structure featuring both macropores and more compact cross-linking clusters. This manifested in the ssNMR as more mobile water molecules and fewer alginate-hydration sites. It is worth noting that these changes likely mostly involve reordering and restructuring of the G monosaccharides, which were generally less visible in the

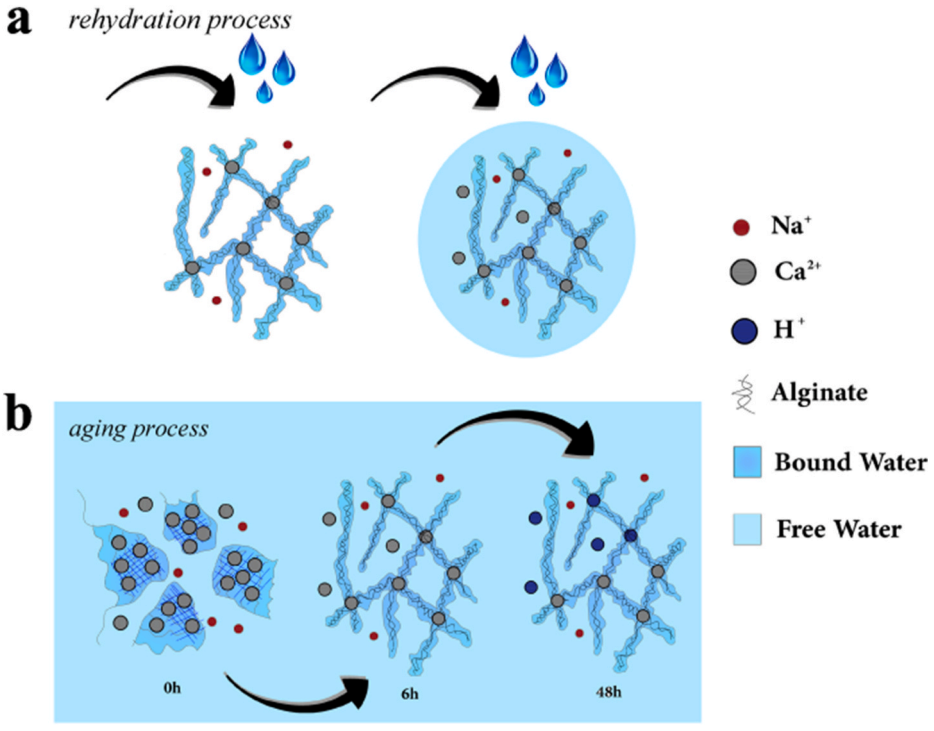

Fig. 11. Schematic overview of the rehydration and aging of alginate hydrogels. (a) Water penetration of lyophilized Ca-cross-linked alginate, showing the observed initial occupation (left) of hydration water sites on the alginate and secondarily the filling of macropores (right), upon saturation of the alginate-interacting sites. (b) Upon the addition of Ca^{2+} ions, alginate rapidly solidifies into a gel form with 71 nm size particles, then upon aging alginate particles restructure into smaller particle sizes, while macropores rearrange along the alginate structure. Upon aging for a longer period competitive exchange between the hydration of the alginate carboxyl functional groups and the Ca-induced cross-linking appear.

^{13}C DE ssNMR spectra, due to their relative rigidity in DE ssNMR. In this, these monosaccharides (involved in eggbox style Ca^{2+} cross-links) clearly differed from the more mobile and hydration-prone M carbons. The observation that the particle size aggregates over time convert into smaller size particles, occurs alongside the opening up of more macropores that dominate the structure of alginate hydrogels. Our results show that under the employed experimental conditions, the aggregation process and (re)positioning of Ca^{2+} ions reached an equilibrium in the first few hours (0–6 h) of aging.

As noted, we observed (Figs. 6, 8 and 10) that the Ca^{2+} cross-linking process leads to a change in the hydration properties. Increasing cross-linking times shifted the hydrogel water away from the bound hydration waters toward more of the macropore water. The latter were the more mobile waters that appear as narrow peaks in ^{1}H (and ^{2}H) NMR spectra, while the former were responsible for the broader peaks. The exact mechanism that unifies the preferential hydration of M-based clusters with the seeming loss of hydration sites upon progressive aging remains uncertain. Our findings suggest that there may be a competition between Ca binding and (re)hydration, such that progressing cross-linking times lead to a reduced capacity for tight binding by hydration waters. Thus, added water is increasingly available for the hydration of macropores in the alginate hydrogel. The aging process mechanism is schematically summarized in Fig. 11b.

This connection between cross-linking, hydration and (alginate) mobility may have practical implications for the various uses of alginate-based materials and hydrogels. It has been noted that a common use for alginate hydrogels is for encapsulating or entrapping guest molecules (ranging from bioactive ingredients to drugs and biologics) (Bennacef et al., 2021; Sanchez-Ballester et al., 2021; Santos & Garcia-Rojas, 2021). The hydration properties of these guest molecules are very important, with prior studies (Forgács et al., 2021; Hoffman, 2012) showing that hydration affects properties such as self-association, aggregation and re-solubilization of these substrates. Moreover, reversible de- and re-hydration is of importance in pharmaceutical and other uses of alginates. The current work provided molecular-level insights into the hydration process from both the alginate and water components' perspective, with these insights enabled in large part by our use of MAS ssNMR. These ssNMR studies build on a growing literature showing the capabilities of this technique for studying hydrogels. In the current work we highlighted the potential for multinuclear methods of MAS NMR to be applied to the hydrogel in various hydration (and dry) states, to study the progressive changes in hydration, dynamics and macropore or mesh sizes. These parameters are important for the drug encapsulation and delivery, as well as other hydrogel applications. We therefore foresee important uses for such ssNMR methods in our own research and more generally, especially in combination with functional and rheological studies, such that one can place macroscopic and functional hydrogel properties on a solid "molecular" footing.

5. Conclusions

The state of water in hydrogels is non-uniform and the arrangement of water molecules in the structure reflects the mesh size and macropore distribution of the hydrogel. These hydrogel parameters play critical roles in understanding and determining properties and behaviors of the hydrogels, such as rheological behavior, in-homogeneity in structure, swelling degree, nutrient and cellular products uptake into the gel, release mechanisms of entrapped molecules, and inject-ability (squeezing behavior through the needle of a syringe) for use in mini-invasive surgery and localized therapy (Cuccia et al., 2020; Haggerty et al., 1988; Kirschner & Anseth, 2013; Pescosolido et al., 2012; Raghuwanshi & Garnier, 2019; Wang & Ugaz, 2006). In this study, two prominent water phases with different relaxation and dynamical properties were detected and characterized in intact rehydrated alginate hydrogels as a function of Ca^{2+} cross-linking. Our characterization of these two water pools with distinguishable properties has relevance to the design of hydrogel properties. The ability to tune and quantify the (macro)pores and hydration waters can provide valuable information about how a hydrogel can capture and integrate food additives and drugs, with also implications for e.g. the diffusion rates for the release of integrated compounds. Finally, the presence and quantity of free water could be linked to bacterial and fungal proliferation in food industry, thus predicting and tuning the shelve life for food products. We observed how an increase in the Ca^{2+} cross-linking period decreased the particle size of alginate nanoparticles, but also impacted the hydration behavior and ratio of macropore-to hydration-water. It was shown that ssNMR offers unique insights that are highly complementary to other characterization techniques, and can therefore be expected to enhance the informed (re)design of biomedically relevant alginate-based materials. An interplay between cross-linking and hydration behavior may offer new means to control the homogeneity, structure and dynamics of the hydrogel architecture, e.g. to control the amount of macropore water, which is relevant for the dissolution and hydration of encapsulated drugs and biologics, and thus crucial for controlled and enhanced drug delivery performance.

CRediT authorship contribution statement

Mustapha El Hariri El Nokab: Conceptualization, Investigation, Formal analysis, Visualization, Writing – original draft. **Alessia Lasorsa:** Investigation, Formal analysis, Visualization. **Khaled O. Sebakhy:** Conceptualization, Investigation, Formal analysis, Visualization. **Francesco Picchioni:** Supervision. **Patrick C.A. van der Wel:** Conceptualization, Supervision, Writing – review & editing, Project administration.

Declaration of interests

The authors declare that they have no known competing financial interests or personal relationships that could have appeared to influence the work reported in this paper.

Acknowledgments

This work was supported by financial support from the Zernike Institute for Advanced Materials at the University of Groningen, including funding from the Bonus Incentive Scheme of the Dutch Ministry for Education, Culture and Science (OCW).

Appendix A. Supplementary data

Supplementary data to this article can be found online at https://doi.org/10.1016/j.foodhyd.2022.107500.

References

Abasalizadeh, F. (2020). Alginate-based hydrogels as drug delivery vehicles in cancer treatment and their applications in wound dressing and 3D bioprinting. *Journal of Biological Engineering, 14*, 22. https://doi.org/10.1186/s13036-020-0227-7

Amsden, B. (1998). Solute diffusion within hydrogels. Mechanisms and models. *Macromolecules, 31*, 8382–8395. https://doi.org/10.1021/ma980765f

Andersen, T., Auk-Emblem, P., & Dornish, M. (2015). 3D cell culture in alginate hydrogels. *Microarrays, 4*, 133–161. https://doi.org/10.3390/microarrays4020133

Atkins, E. D. T., Nieduszynski, I. A., Mackie, W., Parker, K. D., & Smolko, E. E. (1973). Structural components of alginic acid. II. The crystalline structure of poly-a-L-guluronic acid. Results of X-ray diffraction and polarized infrared studies. *Biopolymers, 12*, 1879–1887. https://doi.org/10.1002/bip.1973.360120814

Baumgartner, S., Lahajnar, G., Sepe, A., & Kristl, J. (2002). Investigation of the state and dynamics of water in hydrogels of cellulose ethers by ^{1}H NMR spectroscopy. *AAPS PharmSciTech, 3*, 86. https://doi.org/10.1208/pt030436

Bennacef, C., Desobry-Banon, S., Probst, L., & Desobry, S. (2021). Advances on alginate use for spherification to encapsulate biomolecules. *Food Hydrocolloids, 118*, 106782. https://doi.org/10.1016/j.foodhyd.2021.106782

Bennett, A. E., Rienstra, C. M., Auger, M., Lakshmi, K. V., & Griffin, R. G. (1995). Heteronuclear decoupling in rotating solids. *The Journal of Chemical Physics, 103*, 6951–6958. https://doi.org/10.1063/1.470372

Böckmann, A., Gardiennet, C., Verel, R., Hunkeler, A., Loquet, A., Pintacuda, G., Emsley, L., Meier, B. H., & Lesage, A. (2009). Characterization of different water

pools in solid-state NMR protein samples. *Journal of Biomolecular NMR, 45*, 319–327. https://doi.org/10.1007/s10858-009-9374-3

Braccini, I., & Pérez, S. (2001). Molecular basis of Ca^{2+} -induced gelation in alginates and pectins: The egg-box model revisited. *Biomacromolecules, 2*, 1089–1096. https://doi.org/10.1021/bm010008g

Brus, J., Urbanova, M., Czernek, J., Pavelkova, M., Kubova, K., Vyslouzil, J., Abbrent, S., Konefal, R., Horský, J., Vetchy, D., Vysloužil, J., & Kulich, P. (2017). Structure and dynamics of alginate gels cross-linked by polyvalent ions probed via solid state NMR spectroscopy. *Biomacromolecules, 18*, 2478–2488. https://doi.org/10.1021/acs.biomac.7b00627

Campoccia, D. (1998). Semisynthetic resorbable materials from hyaluronan esterification. *Biomaterials, 19*, 2101–2127. https://doi.org/10.1016/S0142-9612(98)00042-8

Capitani, D., Crescenzi, V., & Segre, A. L. (2001). Water in hydrogels. An NMR study of water/polymer interactions in weakly cross-linked chitosan networks. *Macromolecules, 34*, 4136–4144. https://doi.org/10.1021/ma002109x

Chai, Q., Jiao, Y., & Yu, X. (2017). Hydrogels for biomedical applications: Their characteristics and the mechanisms behind them. *Gels, 3*, 6. https://doi.org/10.3390/gels3010006

Chan, L. W., Ching, A. L., Liew, C. V., & Heng, P. W. S. (2007). Mechanistic study on hydration and drug release behavior of sodium alginate compacts. *Drug Development and Industrial Pharmacy, 33*, 667–676. https://doi.org/10.1080/03639040600943814

Chen, Y. (2018). Preparation of the chitosan/poly(glutamic acid)/alginate polyelectrolyte complexing hydrogel and study on its drug releasing property. *Carbohydrate Polymers, 191*, 9. https://doi.org/10.1016/j.carbpol.2018.02.065

Chivers, P. R. A., & Smith, D. K. (2019). Shaping and structuring supramolecular gels. *Nature Review Materials, 4*, 463–478. https://doi.org/10.1038/s41578-019-0111-6

Cuccia, N. L., Pothineni, S., Wu, B., Méndez Harper, J., & Burton, J. C. (2020). Pore-size dependence and slow relaxation of hydrogel friction on smooth surfaces. *Proceedings of the National Academy of Sciences, 117*, 11247–11256. https://doi.org/10.1073/pnas.1922364117

Dahlmann, J., Krause, A., Möller, L., Kensah, G., Möwes, M., Diekmann, A., Martin, U., Kirschning, A., Gruh, I., & Dräger, G. (2013). Fully defined in situ cross-linkable alginate and hyaluronic acid hydrogels for myocardial tissue engineering. *Biomaterials, 34*, 940–951. https://doi.org/10.1016/j.biomaterials.2012.10.008

Delaglio, F., Grzesiek, S., Vuister, G. W., Zhu, G., Pfeifer, J., & Bax, A. (1995). NMRPipe: A multidimensional spectral processing system based on UNIX pipes. *Journal of Biomolecular NMR, 6*. https://doi.org/10.1007/BF00197809

Dompé, M., Cedano-Serrano, F. J., Vahdati, M., Westerveld, L., Hourdet, D., Creton, C., Gucht, J., Kodger, T., & Kamperman, M. (2020). Underwater adhesion of multiresponsive complex coacervates. *Advanced Materials Interfaces, 7*, 1901785. https://doi.org/10.1002/admi.201901785

El Hariri El Nokab, M., & van der Wel, P. C. A. (2020). Use of solid-state NMR spectroscopy for investigating polysaccharide-based hydrogels: A review. *Carbohydrate Polymers, 240*, 116276. https://doi.org/10.1016/j.carbpol.2020.116276

Forgács, A., Papp, V., Paul, G., Marchese, L., Len, A., Dudás, Z., Fábián, I., Gurikov, P., & Kalmár, J. (2021). Mechanism of hydration and hydration induced structural changes of calcium alginate aerogel. *ACS Applied Materials and Interfaces, 13*, 2997–3010. https://doi.org/10.1021/acsami.0c17012

Friedline, A. W., Zachariah, M. M., Johnson, K., Thomas, K. J., Middaugh, A. N., Garimella, R., Powell, D. R., Vaishampayan, P. A., & Rice, C. V. (2014). Water behavior in bacterial spores by deuterium NMR spectroscopy. *Journal of Physical Chemistry B, 118*, 8945–8955. https://doi.org/10.1021/jp5025119

Fu, R., Wang, X., Li, C., Santiago-Miranda, A. N., Pielak, G. J., & Tian, F. (2011). In situ structural characterization of a recombinant protein in native Escherichia coli membranes with solid-state magic-angle-spinning NMR. *Journal of the American Chemical Society, 133*, 12370–12373. https://doi.org/10.1021/ja204062v

Gidley, M. J. (1992). High-resolution solid-state NMR of food materials. *Trends in Food Science & Technology, 3*, 231–236. https://doi.org/10.1016/0924-2244(92)90197-5

Gidley, M. J., & Bociek, S. M. (1985). Molecular organization in starches: A carbon 13 CP/MAS NMR study. *Journal of the American Chemical Society, 107*, 7040–7044. https://doi.org/10.1021/ja00310a047

Grasdalen, H., Larsen, B., & Smidsrød, O. (1979). A p.m.r. study of the composition and sequence of uronate residues in alginates. *Carbohydrate Research, 68*, 23–31. https://doi.org/10.1016/S0008-6215(00)84051-3

Gun'ko, V. M., Mikhalovska, L. I., Savina, I. N., Shevchenko, R. V., James, S. L., Tomlins, P. E., & Mikhalovsky, S. V. (2010). Characterisation and performance of hydrogel tissue scaffolds. *Soft Matter, 6*, 5351. https://doi.org/10.1039/c0sm00617c

Gun'ko, V., Savina, I., & Mikhalovsky, S. (2017). Properties of water bound in hydrogels. *Gels, 3*, 37. https://doi.org/10.3390/gels3040037

Gun'ko, V. M., Turov, V. V., Bogatyrev, V. M., Zarko, V. I., Leboda, R., Goncharuk, E. V., Novza, A. A., Turov, A. V., & Chuiko, A. A. (2005). Unusual properties of water at hydrophilic/hydrophobic interfaces. *Advances in Colloid and Interface Science, 118*, 125–172. https://doi.org/10.1016/j.cis.2005.07.003

Gun'ko, V. M., Zarko, V. I., Goncharuk, E. V., Andriyko, L. S., Turov, V. V., Nychiporuk, Y. M., Leboda, R., Skubiszewska-Zięba, J., Gabchak, A. L., Osovskii, V. D., Ptushinskii, Y. G., Yurchenko, G. R., Mishchuk, O. A., Gorbik, P. P., Pissis, P., & Blitz, J. P. (2007). TSDC spectroscopy of relaxational and interfacial phenomena. *Advances in Colloid and Interface Science, 131*, 1–89. https://doi.org/10.1016/j.cis.2006.11.001

Haggerty, L., Sugarman, J., & Prudhomme, R. (1988). Diffusion of polymers through polyacrylamide gels. *Polymer, 29*, 1058–1063. https://doi.org/10.1016/0032-3861(88)90015-8

Hecht, H., & Srebnik, S. (2016). Structural characterization of sodium alginate and calcium alginate. *Biomacromolecules, 17*, 2160–2167. https://doi.org/10.1021/acs.biomac.6b00378

Hoffman, A. S. (2012). Hydrogels for biomedical applications. *Advanced Drug Delivery Reviews, 64*, 18–23. https://doi.org/10.1016/j.addr.2012.09.010

Hu, C., Lu, W., Mata, A., Nishinari, K., & Fang, Y. (2021). Ions-induced gelation of alginate: Mechanisms and applications. *International Journal of Biological Macromolecules, 177*, 578–588. https://doi.org/10.1016/j.ijbiomac.2021.02.086

Jhon, M. S., & Andrade, J. D. (1973). Water and hydrogels. *Journal of Biomedical Materials Research, 7*, 509–522. https://doi.org/10.1002/jbm.820070604

Kaieda, S., Setlow, B., Setlow, P., & Halle, B. (2013). Mobility of core water in Bacillus subtilis spores by 2H NMR. *Biophysical Journal, 105*, 2016–2023. https://doi.org/10.1016/j.bpj.2013.09.022

Kay, L. E., Torchia, D. A., & Bax, A. (1989). Backbone dynamics of proteins as studied by nitrogen-15 inverse detected heteronuclear NMR spectroscopy: Application to staphylococcal nuclease. *Biochemistry, 28*, 8972–8979. https://doi.org/10.1021/bi00449a003

Khavari, A., Nydén, M., Weitz, D. A., & Ehrlicher, A. J. (2016). Composite alginate gels for tunable cellular microenvironment mechanics. *Scientific Reports, 6*, 30854. https://doi.org/10.1038/srep30854

Kirschner, C. M., & Anseth, K. S. (2013). Hydrogels in healthcare: From static to dynamic material microenvironments. *Acta Materialia, 61*, 931–944. https://doi.org/10.1016/j.actamat.2012.10.037

Krivokhizhina, T. V., & Wittebort, R. J. (2014). 2Q NMR of 2H2O ordering at solid interfaces. *Journal of Magnetic Resonance, 243*, 33–39. https://doi.org/10.1016/j.jmr.2014.02.022

Kühn, P. T., Meijer, T. L., Schiavon, I., van Poll, M., van Aken, J., Groen, S., Kuijer, R., van Kooten, T. G., & van Rijn, P. (2016). Non-covalently stabilized alginate hydrogels as functional cell scaffold. *Material Macromolecules Bioscience, 16*, 1693–1702. https://doi.org/10.1002/mabi.201600214

Kyritsis, A., Pissis, P., & Grammatikakis, J. (1995). Dielectric relaxation spectroscopy in poly(hydroxyethyl acrylates)/water hydrogels. *Journal of Polymer Science Part B: Polymer Physics, 33*, 1737–1750. https://doi.org/10.1002/polb.1995.090331205

Lee, K. Y., & Mooney, D. J. (2012). Alginate: Properties and biomedical applications. *Progress in Polymer Science, 37*, 106–126. https://doi.org/10.1016/j.progpolymsci.2011.06.003

Li, L., Fang, Y., Vreeker, R., Appelqvist, I., & Mendes, E. (2007). Reexamining the egg-box model in Calcium−Alginate gels with X-ray diffraction. *Biomacromolecules, 8*, 464–468. https://doi.org/10.1021/bm060550a

Lim, F., & Sun, A. (1980). Microencapsulated islets as bioartificial endocrine pancreas. *Science, 210*, 908–910. https://doi.org/10.1126/science.6776628

Lin, X., Ma, Q., Su, J., Wang, C., Kankala, R. K., Zeng, M., … Zhou, S.-F. (2019). Dual-responsive alginate hydrogels for controlled release of therapeutics. *Molecules, 24*, 13. https://doi.org/10.3390/molecules24112089

Li, B., Xu, L., Wu, Q., Chen, T., Sun, P., Jin, Q., … Shi, A.-C. (2007). Various types of hydrogen bonds, their temperature dependence and Water−Polymer interaction in hydrated poly(acrylic acid) as revealed by ^{1}H solid-state NMR spectroscopy. *Macromolecules, 40*, 5776–5786. https://doi.org/10.1021/ma070485c

Mandal, A., Boatz, J. C., Wheeler, T. B., & van der Wel, P. C. A. (2017). On the use of ultracentrifugal devices for routine sample preparation in biomolecular magic-angle-spinning NMR. *Journal of Biomolecular NMR, 67*, 165–178. https://doi.org/10.1007/s10858-017-0089-6

Mandal, A., & van der Wel, P. C. A. (2016). MAS ^{1}H NMR probes freezing point depression of water and liquid-gel phase transitions in liposomes. *Biophysical Journal, 111*, 1965–1973. https://doi.org/10.1016/j.bpj.2016.09.027

Matera, D. L., Wang, W. Y., Smith, M. R., Shikanov, A., & Baker, B. M. (2019). Fiber density modulates cell spreading in 3D interstitial matrix mimetics. *ACS Biomaterials Science & Engineering, 5*, 2965–2975. https://doi.org/10.1021/acsbiomaterials.9b00141

Matlahov, I., & van der Wel, P. C. A. (2018). Hidden motions and motion-induced invisibility: Dynamics-based spectral editing in solid-state NMR. *Methods, 148*, 123–135. https://doi.org/10.1016/j.ymeth.2018.04.015

Mollica, G., Ziarelli, F., Lack, S., Brunel, F., & Viel, S. (2012). Characterization of insoluble calcium alginates by solid-state NMR. *Carbohydrate Polymers, 87*, 383–391. https://doi.org/10.1016/j.carbpol.2011.07.066

Morcombe, C. R., & Zilm, K. W. (2003). Chemical shift referencing in MAS solid state NMR. *Journal of Magnetic Resonance, 162*, 479–486. https://doi.org/10.1016/S1090-7807(03)00082-X

Naohara, R., Narita, K., & Ikeda-Fukazawa, T. (2017). Change in hydrogen bonding structures of a hydrogel with dehydration. *Chemical Physics Letters, 670*, 84–88. https://doi.org/10.1016/j.cplett.2017.01.006

Østberg, T., Vesterhus, L., & Graffner, C. (1993). Calcium alginate matrices for oral multiple unit administration: II. Effect of process and formulation factors on matrix properties. *International Journal of Pharmaceutics, 97*, 183–193. https://doi.org/10.1016/0378-5173(93)90138-6

Pasqui, D., De Cagna, M., & Barbucci, R. (2012). Polysaccharide-based hydrogels: The key role of water in affecting mechanical properties. *Polymers, 4*, 1517–1534. https://doi.org/10.3390/polym4031517

Penfield, M. P., & Campbell, A. M. (1990). Chapter 6 - introduction to food science. In M. P. Penfield, & A. M. Campbell (Eds.), *Experimental food science* (3rd ed., pp. 97–129). San Diego: Academic Press. https://doi.org/10.1016/B978-0-12-157920-3.50010-7.

Pescosolido, L., Feruglio, L., Farra, R., Fiorentino, S., Colombo, I., Coviello, T., Matricardi, P., Hennink, W. E., Vermonden, T., & Grassi, M. (2012). Mesh size distribution determination of interpenetrating polymer network hydrogels. *Soft Matter, 8*, 7708. https://doi.org/10.1039/c2sm25677k

Poulhazan, A., Dickwella Widanage, M. C., Muszyński, A., Arnold, A. A., Warschawski, D. E., Azadi, P., Marcotte, I., & Wang, T. (2021). Identification and quantification of glycans in whole cells: Architecture of microalgal polysaccharides described by solid-state nuclear magnetic resonance. *Journal of the American Chemical Society*. https://doi.org/10.1021/jacs.1c07429, 1c07429.

Prestwich, G. D., Marecak, D. M., Marecek, J. F., Vercruysse, K. P., & Ziebell, M. R. (1998). Controlled chemical modification of hyaluronic acid: Synthesis, applications, and biodegradation of hydrazide derivatives. *Journal of Controlled Release, 53*, 93–103. https://doi.org/10.1016/S0168-3659(97)00242-3

Radloff, D., Boeffel, C., & Spiess, H. W. (1996). Cellulose and cellulose/poly(vinyl alcohol) blends. 2. Water organization revealed by solid-state NMR spectroscopy. *Macromolecules, 29*, 1528–1534. https://doi.org/10.1021/ma950405h

Raghuwanshi, V. S., & Garnier, G. (2019). Characterisation of hydrogels: Linking the nano to the microscale. *Advances in Colloid and Interface Science, 274*, 102044. https://doi.org/10.1016/j.cis.2019.102044

Salomonsen, T., Jensen, H. M., Larsen, F. H., Steuernagel, S., & Engelsen, S. B. (2009a). Direct quantification of M/G ratio from 13C CP-MAS NMR spectra of alginate powders by multivariate curve resolution. *Carbohydrate Research, 344*, 2014–2022. https://doi.org/10.1016/j.carres.2009.06.025

Salomonsen, T., Jensen, H. M., Larsen, F. H., Steuernagel, S., & Engelsen, S. B. (2009b). Alginate monomer composition studied by solution- and solid-state NMR – a comparative chemometric study. *Food Hydrocolloids, 23*, 1579–1586. https://doi.org/10.1016/j.foodhyd.2008.11.009

Salomonsen, T., Jensen, H. M., Stenbæk, D., & Engelsen, S. B. (2008). Chemometric prediction of alginate monomer composition: A comparative spectroscopic study using IR, Raman, NIR and NMR. *Carbohydrate Polymers, 72*, 730–739. https://doi.org/10.1016/j.carbpol.2007.10.022

Salomonsen, T., Jensen, H. M., Stenbæk, D, & Engelsen, S. B. (2008). Rapid determination of alginate monomer compostion using Raman spectroscopy and chemometrics. In P. A. Williams, & G. O. Phillips (Eds.), *Gums and stabilisers for the food industry 14* (pp. 543–551). Cambridge: Royal Society of Chemistry. https://doi.org/10.1039/9781847558312-00543.

Sanchez-Ballester, N. M., Bataille, B., & Soulairol, I. (2021). Sodium alginate and alginic acid as pharmaceutical excipients for tablet formulation: Structure-function relationship. *Carbohydrate Polymers, 270*, 118399. https://doi.org/10.1016/j.carbpol.2021.118399

Santos, M. B., & Garcia-Rojas, E. E. (2021). Recent advances in the encapsulation of bioactive ingredients using galactomannans-based as delivery systems. *Food Hydrocolloids, 118*, 106815. https://doi.org/10.1016/j.foodhyd.2021.106815

Savina, I. N., Gun'ko, V. M., Turov, V. V., Dainiak, M., Phillips, G. J., Galaev, I. Y., & Mikhalovsky, S. V. (2011). Porous structure and water state in cross-linked polymer and protein cryo-hydrogels. *Soft Matter, 7*, 4276. https://doi.org/10.1039/c0sm01304h

Schmitz, K. S., & Lu, M. (1983). Effect of titration charge on the diffusion of bovine serum albumin. *Proceedings of the National Academy of Sciences, 80*, 425–429. https://doi.org/10.1073/pnas.80.2.425

Scholz, I., Hodgkinson, P., Meier, B. H., & Ernst, M. (2009). Understanding two-pulse phase-modulated decoupling in solid-state NMR. *The Journal of Chemical Physics, 130*, 114510. https://doi.org/10.1063/1.3086936

Sederel, L. C., van der Does, L., Beugeling, T., Feijen, J., Bantjes, A., & Kim, S. W. (1983). Comparison of two carboxylate-activating agents for the modification of a synthetic heparinoid polyelectrolyte. *Journal of Polymer Science - Polymer Letters Edition, 21*, 1–11. https://doi.org/10.1002/pol.1983.130210101

Sikorski, P., Mo, F., Skjåk-Bræk, G., & Stokke, B. T. (2007). Evidence for egg-box-compatible interactions in Calcium−Alginate gels from fiber X-ray diffraction. *Biomacromolecules, 8*, 2098–2103. https://doi.org/10.1021/bm0701503

Smaniotto, F., Prosapio, V., Zafeiri, I., & Spyropoulos, F. (2020). Freeze drying and rehydration of alginate fluid gels. *Food Hydrocolloids, 99*, 105352. https://doi.org/10.1016/j.foodhyd.2019.105352

Sosnik, A. (2014). Alginate particles as platform for drug delivery by the oral route: State-of-the-Art. *ISRN Pharm, 1–17*. https://doi.org/10.1155/2014/926157, 2014.

Takka, S., Ocak, Ö. H., & Acartürk, F. (1998). Formulation and investigation of nicardipine HCl–alginate gel beads with factorial design-based studies. *European Journal of Pharmaceutical Sciences, 6*, 241–246. https://doi.org/10.1016/S0928-0987(97)10005-7

Tang, H., & Hills, B. P. (2003). Use of (13)c MAS NMR to study domain structure and dynamics of polysaccharides in the native starch granules. *Biomacromolecules, 4*, 1269–1276. https://doi.org/10.1021/bm0340772

Tønnesen, H. H., & Karlsen, J. (2002). Alginate in drug delivery systems. *Drug Development and Industrial Pharmacy, 28*, 621–630. https://doi.org/10.1081/DDC-120003853

Urbanova, M., Pavelkova, M., Czernek, J., Kubova, K., Vyslouzil, J., Pechova, A., Molinkova, D., Vyslouzil, J., Vetchy, D., & Brus, J. (2019). Interaction pathways and structure–chemical transformations of alginate gels in physiological environments. *Biomacromolecules, 20*, 4158–4170. https://doi.org/10.1021/acs.biomac.9b01052

Wang, T., Jo, H., DeGrado, W. F., & Hong, M. (2017). Water distribution, dynamics, and interactions with alzheimer's β-amyloid fibrils investigated by solid-state NMR. *Journal of the American Chemical Society, 139*, 6242–6252. https://doi.org/10.1021/jacs.7b02089

Wang, T., Phyo, P., & Hong, M. (2016). Multidimensional solid-state NMR spectroscopy of plant cell walls. *Solid State Nuclear Magnetic Resonance, 78*, 56–63. https://doi.org/10.1016/j.ssnmr.2016.08.001

Wang, J., & Ugaz, V. M. (2006). Using in situ rheology to characterize the microstructure in photopolymerized polyacrylamide gels for DNA electrophoresis. *Electrophoresis, 27*, 3349–3358. https://doi.org/10.1002/elps.200500910

Wang, F., Zhang, R., Chen, T., & Sun, P. (2016). 2H solid-state NMR analysis of the dynamics and organization of water in hydrated chitosan. *Polymers, 8*, 149. https://doi.org/10.3390/polym8040149

Wang, X., & Spencer, H. Garth (1998). Calcium alginate gels: Formation and stability in the presence of an inert electrolyte. *Polymer, 39*, 2759–2764. https://doi.org/10.1016/S0032-3861(97)00597-1

Weingarth, M., & Baldus, M. (2013). Solid-state NMR-based approaches for supramolecular structure elucidation. *Accounts of Chemical Research, 46*, 2037–2046. https://doi.org/10.1021/ar300316e

van der Wel, P. C. A. (2017). Insights into protein misfolding and aggregation enabled by solid-state NMR spectroscopy. *Solid State Nuclear Magnetic Resonance, 88*, 1–14. https://doi.org/10.1016/j.ssnmr.2017.10.001

van der Wel, P. C. A. (2018). New applications of solid-state NMR in structural biology. *Emergency Topics in Life Science, 2*, 57–67. https://doi.org/10.1042/ETLS20170088

Wende, F. J., Xue, Y., Nestor, G., Öhrlund, Å., & Sandström, C. (2020). Relaxation and diffusion of water protons in BDDE cross-linked hyaluronic acid hydrogels investigated by NMR spectroscopy—comparison with physicochemical properties. *Carbohydrate Polymers, 248*, 116768. https://doi.org/10.1016/j.carbpol.2020.116768

White, P. B., Wang, T., Park, Y. B., Cosgrove, D. J., & Hong, M. (2014). Water–polysaccharide interactions in the primary cell wall of Arabidopsis thaliana from polarization transfer solid-state NMR. *Journal of the American Chemical Society, 136*, 10399–10409. https://doi.org/10.1021/ja504108h

Yoshida, H., Hatakeyama, T., & Hatakeyama, H. (1993). Characterization of water in polysaccharide hydrogels by DSC. *Journal of Thermal Analysis, 40*, 483–489. https://doi.org/10.1007/BF02546617

Yudianti, R., Karina, M., Sakamoto, M., & Azuma, J. (2009). DSC analysis on water state of salvia hydrogels. *Macromolecular Research, 17*, 1015–1020. https://doi.org/10.1007/BF03218650